Agricultural and Forest Meteorology 290 (2020) 107986

Contents lists available at ScienceDirect

Agricultural and Forest Meteorology

journal homepage: www.elsevier.com/locate/agrformet

A new perspective on the open-path infrared gas analyzer self-heating correction

John M. Frank[a,*,1], William J. Massman[a,1]

[a] USDA Forest Service, Rocky Mountain Research Station, 240 W. Prospect Rd., Fort Collins, CO, 80526, United States

ARTICLE INFO

Keywords:
Eddy covariance
Open-path infrared gas analyzer
Burba correction
Self-heating

ABSTRACT

Across networks of cold weather sites, eddy covariance measurements of ecosystem fluxes commonly indicate carbon uptake throughout winter, a problem that has been linked to open-path infrared gas analyzer (IRGA) self-heating. Though there is no definitive consensus about this phenomenon, the de facto correction for the prevalent LI-7500 is the methodology of Burba et al. (2008) (B08), which predicts self-heating from IRGA surface temperatures and boundary layers. In this paper we examine the validity of this model compared to an updated correction by conducting field studies with the LI-7500 and an IRGA designed by the National Oceanic and Atmospheric Administration (NOAA). Both types of sensors were instrumented to measure sensible heat flux within the instrument path and temperatures of key instrument surfaces. We test hypotheses that (1) considerable IRGA self-heating occurs at a cold, windy, high elevation, mountainous field site, (2) unwarranted boundary layer adjustment terms defined in B08 reduce the bottom and top surface heat fluxes by an order of magnitude, and (3) the weighted sum of the surface heat fluxes should be proportional to their surface area contribution to the IRGA measurement volume. We detected more sensible heat flux within the LI7500 path than outside of it (statistical slopes between 0.95 to 1.3 and offsets between 0 and 35 W m^{-2}) with the largest discrepancies occurring during the day and in winter. The NOAA IRGA has a similar structure to the LI-7500, but with flat surfaces that do not warrant the boundary layer adjustment terms in B08. Bayesian analyses indicated the bottom and top surface heat flux weightings from B08 are improbable and an order of magnitude too large. For the LI-7500, when the boundary layer adjustment terms were omitted the B08 weightings were also improbable; by including these terms and using the new weightings, self-heating estimates were reasonable only because the bottom and top sensible heat fluxes became negligible. We conclude that it is likely the B08 self-heating correction has two errors that roughly cancel out at our field site; this should not generally be expected. The new formulation emphasizes the role of the spar in self-heating, which should be taken into consideration for all cold-weather installations regardless of how the IRGA is mounted.

1. Introduction

Energy and trace gases fluxes between the atmosphere and land surface are fundamental for studies of ecosystem function, ecohydrology, carbon cycling, and climate change. The eddy covariance (EC) technique for measuring fluxes has become commonplace as technological advancements have led to micrometeorological instrumentation that is more accurate and reliable (Baldocchi, 2014). The premise of EC measurements is that the energy and mass that cross the hypothetical boundary dividing the atmosphere from the ecosystem can be measured at high frequency and then tallied over a longer period of time. However, there are non-biological processes that can influence gas exchange across this boundary; most notably due to contraction and expansion of the atmosphere corresponding to the ideal gas law (Webb et al., 1980). Trace gas instruments based on optical absorption intrinsically measure molecular number density, which must be accounted for in order to produce meaningful fluxes. For instruments whose measurement volume are exposed to the atmosphere (i.e., open-path), the Webb-Pearman-Leuning (WPL) correction (Webb et al., 1980) accounts for the non-biological processes, in part, with a sensible heat flux adjustment. As the number of eddy covariance deployments in cold weather sites has expanded, the issue of wintertime EC measurements indicating carbon dioxide uptake (i.e., a winter CO_2 sink) has become apparent (Amiro, 2010). Burba et al. (2008) investigated the cause of this with an

* Corresponding author.
E-mail address: john.frank@usda.gov (J.M. Frank).
[1] This paper was written and prepared by a U.S. Government employee on official time, and therefore it is in the public domain and not subject to copyright.

https://doi.org/10.1016/j.agrformet.2020.107986
Received 9 August 2019; Received in revised form 16 March 2020; Accepted 22 March 2020
0168-1923/ Published by Elsevier B.V.

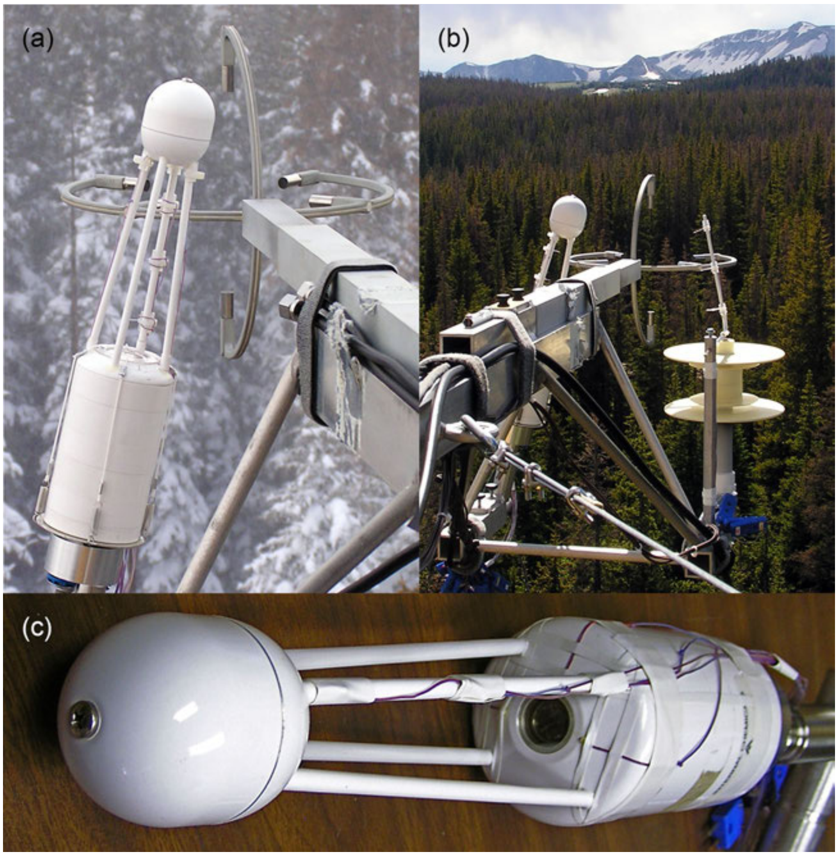

Fig. 1. The LI-7500 study with (a, 29 January 2009) thermocouples mounted on the bottom, spar, and top surfaces with three more protruding from the spar used for eddy covariance measurements of S^{path}, (b, 13 July 2010) three thermocouples mounted on a white metal rod on the other side of the sonic anemometer and used for eddy covariance measurements of S^{out}, and (c, 30 August 2013) bottom and spar surface temperature measurements using thermocouples affixed with white vinyl tape. The study was conducted at the Glacier Lakes Ecosystem Experiments Site (GLEES) in Wyoming, USA.

open-path infrared gas analyzer (IRGA), the LI-7500 (Li-Cor, Inc., Lincoln, NE, USA, Fig. 1), which operates with warm surfaces that contribute additional sensible heat flux to the WPL correction (Lee and Massman, 2011). Since then, numerous studies have investigated the implications of the self-heating correction over broader networks of eddy covariance sites and the use of open-path IRGAs is generally correlated with biased wintertime CO_2 fluxes (Reverter et al., 2011; Wang et al., 2017b); whether this is entirely due to self-heating is debatable (Wang et al., 2017a).

Burba et al. (2006) proposed a self-heating correction which estimated the additional heat flux from the temperature gradient between the IRGA and the ambient air with an aerodynamic resistance formulation. Their approach incorporates a weighting multiplier based on the fraction of the surface heat flux retained in the optical path; this value was allowed to vary and was assumed to change with different instrument orientations. Rogiers et al. (2008) and Järvi et al. (2009) expanded upon this approach, with the later using the fraction term as a way to empirically fit the eddy covariance data from open- and closed-path sensors. These studies have provided an approach to correct for self-heating (Zweifel et al., 2010) and to compare open- and closed-path eddy covariance measurements (Holl et al., 2019; Kittler et al., 2017).

The methodology of Burba et al. (2008) revised this approach and has since become the de facto correction for LI-7500 self-heating. Conceptually, the additional IRGA heat flux is determined in two steps: a first principles based model that predicts self-heating from the surface to atmosphere temperature gradients and surface boundary layers plus an empirical model predicting the surface temperatures from ambient meteorology. It is common for the unaltered Burba et al. (2008) correction to be applied at flux sites (Blanken et al., 2009; Euskirchen et al., 2012; Galvagno et al., 2013; Marushchak et al., 2013; Miller et al., 2011; Sturtevant and Oechel, 2013; Webb et al., 2016) and to be used to compare open- and closed-path EC measurements (Euskirchen et al., 2017; Ueyama et al., 2012). It has also been applied to an entirely different IRGA (Ikawa et al., 2013). Some studies have modified the correction for their specific sites through direct measurements of surface temperatures (Nordbo et al., 2012) or by using simultaneous open- and closed-path measurements to build a site specific self-heating correction (Lafleur and Humphreys, 2018). Sometimes self-heating is disregarded by assuming it is negligible for horizontally inclined IRGAs (Lüers et al., 2014); though Oechel et al. (2014) accounted for this by blending the top and bottom surface temperatures while Kittler et al. (2017) dealt with inclination by applying the fraction term from Rogiers et al. (2008) and Järvi et al. (2009) to the Burba et al. (2008) correction. Otherwise, EC data with wintertime CO_2 uptake (Brown et al., 2010; Mathys et al., 2013) or below freezing temperatures (Amiro et al., 2010) have been removed to avoid the issue.

While the evidence in Burba et al. (2008) clearly supports that there is considerable self-heating in the LI-7500 path that corresponds with warmer IRGA surface temperatures, their first principles based model that combines surface temperatures and boundary layers to estimate the self-heating term is inadequately tested. To address this, we conducted two field studies using two different IRGAs instrumented to measure the sensible heat flux within the instrument path as well as the temperatures of key instrument surfaces. We used these studies to evaluate the following hypotheses: (1) IRGA self-heating is considerable at a cold, windy, high elevation, mountainous field site; (2) The bottom and top surface boundary layer definitions in Burba et al. (2008) contain unwarranted constant adjustment terms, which lead to surface heat fluxes which are an order of magnitude less than should be expected; (3) The weighted sum of surface heat fluxes should be proportional to their contribution to the surface area of the IRGA measurement volume; consequently the bottom and top surface weightings in Burba et al. (2008) are an order of magnitude too large.

2. Methods

2.1. The IRGA self-heating correction

The sensible heat flux, S (W m^{-2}), within the IRGA path is:

$$S^{path} = \rho C_p \overline{w'T_a'} + \Delta S \quad (1)$$

where the first term on the right is the sensible heat flux of ambient air and the second term, ΔS (W m^{-2}), is the heat flux contributed from the IRGA (i.e., self-heating); ρ is the air density (kg m^{-3}), C_p is the specific heat of air (J kg^{-1} K^{-1}), and $\overline{w'T_a'}$ is the covariance between vertical wind velocity, w (m s^{-1}), and ambient air temperature, T_a (°C). The most commonly accepted methodology to account for LI-7500 self-heating was proposed by Burba et al. (2008), whose Method 4 estimated IRGA self-heating as a weighted sum of sensible heat fluxes from key instrument surfaces: bottom window, top window, and spar. In this paper we investigate the importance of S^{path} being a function of the average thicknesses of the boundary layer above the key surfaces, δ, as well as weighting parameters, ω, such that we write the Burba et al. (2008) correction in the general form:

$$\begin{aligned} S^{path}(\delta, \omega) &= \rho C_p \overline{w'T_a'} + \omega^{bot} S^{bot}(\delta^{bot}) + \omega^{top} S^{top}(\delta^{top}) + \omega^{spar} S^{spar}(\delta^{spar}) \\ &= \rho C_p \overline{w'T_a'} + \Delta S^{surf}(\delta, \omega) \end{aligned} \quad (2)$$

We define ΔS^{surf} as the weighted sum of the sensible heat fluxes from the instrument surfaces. Throughout our paper we add notation to clarify (1) terms defined by Burba et al. (2008) as "B08", defined by our new formulation with a "^", or empirically estimated from Bayesian analysis as "posterior", (2) key surfaces as "bot", "top", and "spar" with the sum of their sensible heat fluxes as "surf", the volume within the IRGA "path" versus "out" of the path, and sensible heat flux measured with eddy-covariance as "EC", and (3) the type of IRGA, either "LI7500" or "NOAA" (Auble and Meyers, 1992). When any of these subcategories is not specified it is assumed the term is universally applicable for this study. Where there is ambiguity concerning which definitions of δ and ω are used to evaluate a sensible heat flux then the functional notation (δ,ω) is included.

The Burba et al. (2008) correction is defined as the following. First, S within the path of a LI-7500 is estimated as:

$$\begin{aligned} S_{B08}^{path,LI7500} &= \rho C_p \overline{w'T_a'} + \omega_{B08}^{bot} S_{B08}^{bot,LI7500} + \omega_{B08}^{top} S_{B08}^{top,LI7500} + \omega_{B08}^{spar,LI7500} S^{spar} \\ &= \rho C_p \overline{w'T_a'} + S_{B08}^{bot,LI7500} + S_{B08}^{top,LI7500} + 0.15 S^{spar} \\ &= \rho C_p \overline{w'T_a'} + \Delta S_{B08}^{surf,LI7500} \end{aligned} \quad (3)$$

The sensible heat flux from the bottom window, S^{bot} (W m^{-2}), is:

$$S_{B08}^{bot,LI7500} = k^{air} \frac{(T_s^{bot} - T_a)}{\delta_{B08}^{bot,LI7500}} \quad (4)$$

k^{air} is the thermal conductivity of air (W m^{-1} K^{-1}), T_s^{bot} is the temperature of the bottom window (°C), we define ΔT^{bot} as T_s^{bot} - T_a, and the average thickness of the boundary layer above the bottom window, δ^{bot} (m), is:

$$\delta_{B08}^{bot,LI7500} = 0.004\sqrt{\frac{l^{bot}}{U}} + 0.004 \quad (5)$$

l^{bot} is the diameter of the source housing (0.065 m) and U is the ambient horizontal wind speed (m s^{-1}). The sensible heat flux from the top window, S^{top} (W m^{-2}), is:

$$S_{B08}^{top,LI7500} = k^{air} \frac{(r^{top} + \delta_{B08}^{top,LI7500})(T_s^{top} - T_a)}{r^{top}\delta_{B08}^{top,LI7500}} \quad (6)$$

T_s^{top} is the temperature of the top window (°C), r^{top} is the radius of the detector sphere (0.0225 m), we define ΔT^{top} as T_s^{top} - T_a, and the average thickness of the boundary layer below the top window, δ^{top} (m), is:

$$\delta_{B08}^{top,LI7500} = 0.0028\sqrt{\frac{l^{top}}{U}} + \frac{0.00025}{U} + 0.0045 \quad (7)$$

l^{top} is the diameter of the detector housing (0.045 m). The sensible heat flux from the spar, S^{spar} (W m^{-2}), is:

$$S^{spar} = k^{air} \frac{(T_s^{spar} - T_a)}{r^{spar} \ln\left(\frac{r^{spar} + \delta^{spar}}{r^{spar}}\right)} \quad (8)$$

T_s^{spar} is the temperature of the spar (°C), r^{spar} is the radius of the spar cylinder (0.0025 m), we define ΔT^{spar} as T_s^{spar} - T_a, and the average thickness of the boundary layer around the spar, δ^{spar} (m), is:

$$\delta^{spar} = 0.0058\sqrt{\frac{l^{spar}}{U}} \quad (9)$$

l^{spar} is the diameter of the spar (0.005 m).

These equations are adapted from Nobel (1983), who derived the heat fluxes from "plant parts such as stems, branches, inflorescences, fruits, and even certain leaves". Equations 4 and 5 are adapted from the heat flux from a leaf where their l refers to the "length of a leaf in the direction of the wind"; though, the equivalent to Eq. 4 in Nobel (1983) has a factor of 2 (i.e., heat conduction from both sides of the leaf) and the equivalent to Eq. 5 does not have the rightmost constant 0.004, which was added by Burba et al. (2008) to compensate for the 20° bevel surrounding the bottom window of the LI-7500. Equations 6 and 7 are adapted from Nobel (1983) for a sphere; though their equivalent to Eq. 7 does not have the rightmost constant 0.0045, which was added in B08 "to compensate for the nonspherical surface of the top window". Equations 8 and 9 are essentially identical to Nobel (1983) for a cylinder. The constants 0.004 m and 0.0045 m in B08 are the approximate depths of the round surfaces removed from the lower cone and upper sphere to accommodate the flat lenses (G. Burba personal communications, March 2015). It is assumed that air will continue to flow on its curved path around the orb and the airspace within this void will not mix, resulting in an increased boundary layer thickness. The 0.15 coefficient for S^{spar} in Eq. 3 is the probability for a random direction that a plume from the spar would enter the cell path (G. Burba personal communications, March 2015).

2.2. An updated formulation for the IRGA self-heating correction

The additional boundary layer constant in Eq. 5 assumes that air flowing up the 20° bevel of the bottom of the LI-7500 will separate from the surface due to the transition to the flat window, resulting in a boundary layer that grows by an order of magnitude. Without a specific investigation of turbulent air flow across the LI-7500 structure, analogous problems such as boundary layer flows over hills can be used evaluate the validity of this assumption. Though hills are of a dramatically larger scale, when they are studied as non-dimensional objects their results can be applicable to the IRGA problem. Two main benefits of hill studies are they focus on turbulent atmospheric flows and they are often modeled as shapes similar to the bottom of the LI-7500 (Wood, 1995). In these studies, the critical angle where air flow separates from a hill often occurs around 15° (Wood, 1995), though in the case of an 18° slope, separation does not occur until over halfway down the leeward side (Huang, 2015). If these results are analogous to the LI-7500, then separation is likely most pronounced on the leeward 20° bevel after air flows across the window. In this circumstance, it is justified to question the validity of the additional constant in Eq. 5.

The weighting factor associated with $S_{B08}^{bot,LI7500}$ in Eq. 3 assumes that the sensible heat flux contributed from the bottom surface does not

Fig. 2. The NOAA IRGA installed as part of the main GLEES eddy covariance system on 24 January 2006. The 2010 study was conducted on a replicate system mounted 2 m below.

diminish as it propagates throughout the entire measurement volume. As shown in Burba et al. (2008), between 30-50% of the temperature gradient between the surface and ambient air occurs within the first 1 mm of airspace. A laboratory study of an 87 mm diameter heated plate under laminar flow showed that an entire temperature gradient generally does not extend beyond a few millimeters (Willman and Ewart, 2016). Thus, gradient estimates of the sensible heat flux contributed by the bottom surface throughout most of the measurement path will be significantly diminished. While it may be difficult to determine the most appropriate weighting factor, it is justified to question the validity that its values is near 1.

Therefore, we test two changes to the B08 self-heating correction. First, similar to Nobel (1983), the constants are omitted from the boundary layer depths such that δ^{bot} and δ^{top} become:

$$\hat{\delta}^{bot} = 0.004\sqrt{\frac{l^{bot}}{U}} \tag{10}$$

$$\hat{\delta}^{top,LI7500} = 0.0028\sqrt{\frac{l^{top}}{U}} + \frac{0.00025}{U} \tag{11}$$

And similar to Eqs. 4 and 6 we have:

$$\hat{S}^{bot} = k^{air}\frac{(T_s^{bot} - T_a)}{\hat{\delta}^{bot}} \tag{12}$$

$$\hat{S}^{top,LI7500} = k^{air}\frac{\left(r^{top} + \hat{\delta}^{top,LI7500}\right)(T_s^{top} - T_a)}{r^{top}\hat{\delta}^{top,LI7500}} \tag{13}$$

Thus, it is assumed that turbulent air flow will mix down to the surface of both windows, regardless of the irregular shapes caused by the flat windows being embedded within the instrument's curved surfaces. Second, $\hat{\omega}$ are defined a priori as the proportion of the surface area of measurement volume, A^{path} (m^2), that is contributed by the individual surfaces, A^{bot} (m^2), A^{top} (m^2), and A^{spar} (m^2), such that $\hat{\omega}^{bot} = A^{bot}/A^{path}$, $\hat{\omega}^{top} = A^{top}/A^{path}$, and $\hat{\omega}^{spar} = A^{spar}/A^{path}$. To calculate these surface areas, we define a conical frustum volume (i.e. a cone with the tip cut off) where the height is the LI-7500 path length (0.1268 m), the radius of the bottom surface is the distance parallel to the bottom window from its center to the spar center (0.0252 m), and the radius of the top surface is the distance parallel to the top window from its center to the spar center (0.0144 m). $A^{path,LI7500}$ is the surface area of the conical frustum, $A^{bot,LI7500}$ is the surface area of its bottom, $A^{top,LI7500}$ is the surface area of its top, and $A^{spar,LI7500}$ is the projected area of the four spars on the frustum lateral surface area (i.e., $4l^{spar}s$, where the slant height, s, of the frustum is $\sqrt{(0.0252 - 0.0144)^2 + 0.1268^2} = 0.1273$ m). Based on these dimensions, the new formulation for the weighted sum of the sensible heat fluxes of a LI-7500 is

$$\begin{aligned}\hat{S}^{path,LI7500} &= \rho C_p\overline{w'T_a'} + \hat{\omega}^{bot,LI7500}\hat{S}^{bot} + \hat{\omega}^{top,LI7500}\hat{S}^{top,LI7500} + \hat{\omega}^{spar,LI7500}S^{spar}\\ &= \rho C_p\overline{w'T_a'} + 0.108\hat{S}^{bot} + 0.035\hat{S}^{top,LI7500} + 0.225S^{spar}\\ &= \rho C_p\overline{w'T_a'} + \Delta\hat{S}^{surf,LI7500}\end{aligned} \tag{14}$$

To test our hypotheses we define two other weighted sums that are functions of the B08 and new formulations:

$$\begin{aligned}S^{path,LI7500}(\hat{\delta}, \omega_{B08}) &= \rho C_p\overline{w'T_a'} + \omega_{B08}^{bot}\hat{S}^{bot} + \omega_{B08}^{top}\hat{S}^{top,LI7500} + \omega_{B08}^{spar,LI7500}S^{spar}\\ &= \rho C_p\overline{w'T_a'} + \hat{S}^{bot} + \hat{S}^{top,LI7500} + 0.15S^{spar}\\ &= \rho C_p\overline{w'T_a'} + \Delta S^{surf,LI7500}(\hat{\delta}, \omega_{B08})\end{aligned} \tag{15}$$

$$\begin{aligned}S^{path,LI7500}(\delta_{B08}, \hat{\omega}) &= \rho C_p\overline{w'T_a'} + \hat{\omega}^{bot,LI7500}S_{B08}^{bot,LI7500} + \hat{\omega}^{top,LI7500}S_{B08}^{top,LI7500} + \hat{\omega}^{spar,LI7500}S^{spar}\\ &= \rho C_p\overline{w'T_a'} + 0.108S_{B08}^{bot,LI7500} + 0.035S_{B08}^{top,LI7500} + 0.225S^{spar}\\ &= \rho C_p\overline{w'T_a'} + \Delta S^{surf,LI7500}(\delta_{B08}, \hat{\omega})\end{aligned} \tag{16}$$

We also investigate the self-heating correction from an IRGA developed by the National Oceanic and Atmospheric Administration (NOAA) (Auble and Meyers, 1992). It has a similar shape as the LI-7500, except the spars are not tilted and the bottom and top surfaces are flat (Fig. 2). Because of this, Eq. 10 is used with $l^{bot} = 0.0892$ m and the top is similarly defined as:

$$\hat{\delta}^{top,NOAA} = 0.004\sqrt{\frac{l^{top}}{U}} \tag{17}$$

where $l^{top} = 0.0792$ m. The heat flux from the top is similarly from a flat surface:

$$\hat{S}^{top,NOAA} = k^{air}\frac{(T_s^{top} - T_a)}{\hat{\delta}_{NOAA}^{top}} \tag{18}$$

Because of its different geometry, the value $\omega_{B08}^{spar,LI7500} = 0.15$ is not appropriate for the NOAA IRGA. Instead $\hat{\omega}^{spar,NOAA}$ was determined from $A^{spar,NOAA}/A^{path,NOAA}$ by assuming the volume of air within the measurement path is a cylinder with height of 0.20 m and radius 0.0322 m and with four 0.0097 m diameter spars. Consistent with our new formulation of the LI-7500 correction, we define a weighted sum of surface fluxes for the NOAA IRGA where $\hat{\omega}^{bot,NOAA} = A^{bot,NOAA}/A^{path,NOAA}$ and $\hat{\omega}^{top,NOAA} = A^{top,NOAA}/A^{path,NOAA}$ such that:

$$\begin{aligned}\hat{S}^{path,NOAA} &= \rho C_p \overline{w'T_a'} + \hat{\omega}^{bot,NOAA}\hat{S}^{bot} + \hat{\omega}^{top,NOAA}\hat{S}^{top,NOAA} + \hat{\omega}^{spar,NOAA}S^{spar} \\ &= \rho C_p \overline{w'T_a'} + 0.069\hat{S}S^{bot} + 0.069\hat{S}S^{top,NOAA} + 0.261S^{spar} \\ &= \rho C_p \overline{w'T_a'} + \Delta\hat{S}^{surf,NOAA} \end{aligned} \tag{19}$$

To test our hypotheses, we also define a weighted sum of surface fluxes for the NOAA IRGA similar to B08 by combining $\omega_{B08}^{bot} = \omega_{B08}^{top} = 1$ with $\hat{\omega}^{spar,NOAA}$:

$$\begin{aligned}S^{path,NOAA}(\hat{\delta}, \omega_{B08}, \hat{\omega}) &= \rho C_p \overline{w'T_a'} + \omega_{B08}^{bot}\hat{S}^{bot} + \omega_{B08}^{top}\hat{S}^{top,NOAA} + \hat{\omega}^{spar,NOAA}S^{spar} \\ &= \rho C_p \overline{w'T_a'} + \hat{S}^{bot} + \hat{S}^{top,NOAA} + 0.261S^{spar} \\ &= \rho C_p \overline{w'T_a'} + \Delta S^{surf,NOAA}(\hat{\delta}, \omega_{B08}, \hat{\omega}) \end{aligned} \tag{20}$$

2.3. Field measurements

Field observations were made at the Glacier Lakes Ecosystem Experiments Site (GLEES) US-GLE AmeriFlux site (ameriflux.lbl.gov). GLEES is a high elevation subalpine Engelmann spruce (*Picea engelmannii*)-subalpine fir (*Abies lasiocarpa*) forest in the Snowy Range mountains of southeastern Wyoming, USA. The ~23 m scaffold rises above a canopy that averages ~7 m, reaches ~18 m height, and was recently defoliated from a spruce beetle (*Dendroctonous rufipennis*) outbreak (Frank et al., 2014). The scaffold is located at 41.3665° N and 106.2400° W at 3190 m elevation above sea level. The main US-GLE eddy covariance system includes a sonic anemometer (3Vx probe, Applied Technologies, Inc., Longmont, CO, USA) mounted at 22.65 m on a boom pointed due west with a LI-7500 mounted 0.24 m east, 0.08 m south of the anemometer, and tilted northwards by ~15° from vertical; the centers of the anemometer and IRGA paths were vertically aligned. We use the US-GLE micrometeorological data as ancillary data for this study. Additional description and detail about the GLEES site are in Musselman (1994) and about the US-GLE micrometeorological measurements are in Frank et al. (2014) and Frank et al. (2019).

2.3.1. Measurements of IRGA surface temperatures

The IRGA self-heating correction based on Method 4 of Burba et al. (2008) requires knowledge of the temperatures of the key surfaces of the LI-7500. Beginning in January 2009, thermocouples (36 AWG type-T thermocouple wire, thermojunctions soldered and trimmed to ~1 mm, and insulated with Omegabond 101, Omega Engineering, Inc., Stamford, CT, USA) were secured to the surface near the bottom window, on one spar, and near the upper window (Fig. 1). Three thermocouples were compressed against the surface near the bottom window and 90° apart from each other by a flat plastic ring that was under tension by springs attached to the bottom of the analyzer. Three thermocouples were compressed against the spar along every quarter of its length by ~13 mm pieces of clear tubing (6.35 mm OD x 3.17 mm ID, i.e., 1/4” OD x 1/8” ID, Bev-A-Line IV, Thermoplastic Processes, Inc., Georgetown, DE, USA) that were split lengthwise, wrapped around the spar, and compressed with a wire tie. Finally, three thermocouples were secured against the surface near the top window by compressing them under smaller pieces of clear tubing that were wrapped around the tops of three of the spars and compressed with a wire tie. All of the thermojunctions were partially exposed to the atmosphere. In October 2013, the spring loaded ring and clear tubing were removed, and thereafter thermocouples were secured with white vinyl electrical tape (19 mm, i.e. 3/4”, 35 White, 3M, Austin, TX, USA) (Fig. 1c). Starting in March 2011 the thermocouples around the top window were removed. Three different LI-7500s were deployed during these field measurements: S/N 75-0235 (constructed in 2001) from January 2009 to July 2009 and June 2010 to March 2011, S/N 75-1259 (constructed in 2007) from July 2009 to June 2010, and S/N 75-1751 (constructed in 2009) from March 2011 to June 2014. All of these sensors pre-date the LI-7500A which generally operates at lower internal temperatures (Burba, 2013).

Though the NOAA IRGA was deployed at the US-GLE site from January-February 2006 and on the older US-GBT AmeriFlux tower from November 1999 to January 2006, surface temperatures were never measured at this time. Instead, a second eddy covariance system with similar equipment as the main system was mounted at 20.7 m on the US-GLE scaffold from January to July 2010. During this time, thermocouples were mounted in a similar manner with three located near the bottom window, three mounted on a spar, and three near the top mirror; the bottom and top thermocouples were epoxied in place while the spar thermocouples were taped.

2.3.2. Measurements of sensible heat flux within the IRGA path

Beginning in January 2009, thermocouples were attached to a spar to measure the temperature within the path of the LI-7500 in order to determine the sensible heat flux due to IRGA self-heating. Corresponding to the location of the three spar surface thermocouples, three more thermocouples were added, each one wrapped around the exterior of the ~13 mm tubing pieces, and extending ~10 mm past the spar towards the optical path (Fig. 1a). The thermocouples were of the same specifications as the surface temperatures, except the Omegabond 101 was not applied; this was done to decrease the time constant of the 36 AWG thermocouple from ~0.3 s to ~0.05 s or equivalently increase the frequency response from ~3 Hz to ~20 Hz (experimental results obtained from dipping thermocouples into ice water are not shown). After preliminary data were collected, it was determined that the thermocouple frequency response was dampened compared to the sonic anemometer virtual temperature. Thus, in July 2010 a second array of thermocouples was added as a control; they were located outside of the path on the opposite side of the sonic anemometer and mounted on a white metal rod that was 0.0042 m diameter and 0.15 m long (i.e., dimensions that roughly mimic a LI-7500 spar) and tilted southwards by ~15° from vertical (Fig. 1b). We used the eddy covariance technique to determine $S^{path,LI7500}$ and S^{out} and processed the data in the same manner of the US-GLE dataset: i.e., data collected at 20 Hz, processed each half hour, median despiked (Frank et al., 2014), screened for quality assurance/quality control (Vickers and Mahrt, 1997), rotated into planar-fit coordinates (Lee et al., 2004), time lag adjusted, and spectrally corrected (Massman, 2000). The notable difference is the US-GLE sensible heat flux corrects the sonic anemometer virtual temperature for the buoyancy component from moisture flux (Massman and Lee, 2002), which is unnecessary for the thermocouple measurements. We defined ΔS_{EC} from these measurements as $S^{path,LI7500}$ - S^{out}. The within-path thermocouples were removed in March 2011 and those outside of the path removed in July 2012.

For the NOAA IRGA, three thermocouples were similarly mounted from January to July 2010 on one spar to measure the temperature within the path; no thermocouples were mounted outside of the path. For the NOAA IRGA we defined ΔS_{EC} as $S^{path,NOAA}$ - S^{sonic} where the US-GLE sonic anemometer provided the heat flux outside of the path.

2.4. Statistical analyses

We conducted two statistical analyses on the LI-7500 and one on the NOAA IRGA. For the LI-7500, first, we tested whether or not the sensible heat flux within the measurement path was significantly larger than outside the path. Second, we analyzed the effect of boundary layer definitions (δ_{B08} versus $\hat{\delta}$, i.e., the ramifications of the 0.004 m and 0.0045 m boundary layer adjustment terms for non-flat surfaces) and weightings (i.e., $\omega_{B08}^{bot} = \omega_{B08}^{top} = 1$ versus $\hat{\omega}^{bot,LI7500} = 0.108$ and $\hat{\omega}^{top,LI7500} = 0.035$) on the accuracy of the sum of surface heat fluxes to predict the eddy covariance measurements of self-heating. We used Bayesian analyses to estimate the weightings given a set of surface boundary layer definitions. For the NOAA IRGA, we analyzed the effect of weightings (i.e., $\omega_{B08}^{bot} = \omega_{B08}^{top} = 1$ versus $\hat{\omega}^{bot,NOAA} = \hat{\omega}^{top,NOAA} = 0.069$) on the accuracy of the sum of surface heat fluxes to predict the eddy covariance measurements of self-heating. We interpret weightings as probable if their values occur within the 95% credible intervals of the Bayesian posterior distribution (Lu et al., 2012) and improbable if they do not. The analyses were limited to 30 minute periods where all replicate surface and path thermocouples were operational.

All analyses were performed using Bayesian statistics using Markov chain Monte Carlo (MCMC) methods (Kruschke, 2014). For the first LI-7500 analysis, our statistical model predicted the half-hourly eddy covariance data from six thermocouples (i.e., three in the path and three outside the path) as a set of normal distributions. The means of these normal distributions were defined as S^{out} for the heat flux outside the path and as $mS^{out} + b$ for the heat flux inside the path, where S^{out} is a set of process parameters representing the "true" ambient heat flux for each half-hour and m and b are slope and offset parameters. The role of environmental covariates on m and b was evaluated, with the following covariates chosen using a modified deviance information criterion (Spiegelhalter et al., 2002): day/night, wind speed, ambient temperature (day only), and wind direction (θ in units of °, not including the offset at night). The environmental covariates were scaled such that U and T_a were divided by their standard deviations, the cosine of θ was used in the analysis, and day was determined as downwelling shortwave radiation > 5 W m^{-2}. Though U and T_a were not scaled by the standard z-transformation, the only practical differences were in the parameters associated with the categorical variables day and night; since we only interpret daytime versus nighttime heating relative to the combination of all environmental variables, these differences have no effect on the interpretation of our results. The predicted heat fluxes were also adjusted for random slope and offset effects associated with each of the six thermocouples. The standard deviations of these normal distributions shared a common process parameter that was adjusted for heteroscedasticity.

The second LI-7500 analysis was performed in two steps. In the first step, our statistical model predicted the half-hourly S data from the 15 thermocouples (i.e., the six eddy covariance measurements from inside and outside the path plus the nine derived for the bottom, top, and spar surfaces including the different formulations of $S_{B08}^{bot,LI7500}$, $S_{B08}^{top,LI7500}$, $\hat{S}^{bot}$, and $\hat{S}^{top,LI7500}$) as sets of normal distributions. The means of these normal distributions were sets of process parameters representing the "true" S^{path}, S^{out}, S^{bot}, S^{top}, and S^{spar} with adjustments for random slope and offset effects associated with the replicate thermocouples. The predictions of S^{path} and S^{out} shared the same standard deviation and heteroscedasticity process parameters while S^{bot}, S^{top}, and S^{spar} each had their own. Even though ΔS_{EC} is not defined as a set of process parameters, it is a set of posterior derived quantities calculated from S^{path} - S^{out} from which statistical inferences can also be made Hobbs and Hooten, 2015). The second step investigated different weightings of the surface heat fluxes. Our statistical model predicted the derived quantity ΔS_{EC} as a set of normal distributions with means equal to weighted sums of two sets process parameters: $S_{B08}^{bot,LI7500}$, $S_{B08}^{top,LI7500}$, and S^{spar} versus $\hat{S}^{bot}$, $\hat{S}^{top,LI7500}$, and S^{spar}. For these analyses we defined the process parameters ω^{bot}, ω^{top}, and ω^{spar} with prior probability distributions based on Eq. 3 (see Appendix A.). Because of the difficulty of using a statistical model to separate sensible heat flux into three sources, it is reasonable to expect that some realistic weightings may occur outside the 95% credible intervals and thus be considered improbable; decomposing sensible heat flux into fewer sources could expand these parameter estimates. As the conceptual difference between the B08 and new weightings is focused on ω^{bot} and ω^{top} (i.e., Eqs. 3 and (14), we desire to evaluate a robust range of plausible weightings for the bottom and top surfaces. To do this, we performed the analyses with the Bayesian cut function applied to the ω^{spar} parameter. The Bayesian cut function limits the flow of information between process parameters Plummer, 2015a), which in this case allowed the posterior of ω^{spar} to vary according to its prior distribution and essentially allows the statistical model evaluate ω^{bot} and ω^{top} as if ω^{spar} was constant. Thus, we conducted four weighting analyses: ((1) predicting ΔS_{EC} from $S_{B08}^{bot,LI7500}$, $S_{B08}^{top,LI7500}$, and S^{spar} and obtaining the posterior derived quantity $\Delta S^{surf,LI7500}(\delta_{B08}, \omega_{posterior})$, (2) predicting ΔS_{EC} from $S_{B08}^{bot,LI7500}$, $S_{B08}^{top,LI7500}$, and S^{spar} with the Bayesian cut function applied to ω^{spar}, (3) predicting ΔS_{EC} from $\hat{S}^{bot}$, $\hat{S}^{top,LI7500}$, and S^{spar} and obtaining the posterior derived quantity $\Delta S^{surf,LI7500}(\hat{\delta}, \omega_{posterior})$, and (4) predicting ΔS_{EC} from $\hat{S}^{bot}$, $\hat{S}^{top,LI7500}$, and S^{spar} with the Bayesian cut function applied to ω^{spar}. Finally, in our preliminary results S^{out} was ~20% smaller than S^{sonic} from the US-GLE sonic anemometer. We assumed that this was due to a dampened thermocouple frequency response. Our ice-bath tests indicated the time constant of un-epoxied thermocouples is short, and the spectral corrections applied to our eddy covariance measurements to account for this were negligible. It is possible that in our field study the effective time constant was considerably longer due to the metal spar acting as a thermal dampener to the attached thermocouple wire; in the ice bath the thermojunction and a sizeable amount of thermocouple wire were both immersed together with limited contact to any other surface that could dampen the response. To account for this potential error, a thermocouple adjustment was applied to ΔS_{EC} that was obtained from the slope of the S^{out} versus S^{sonic} reduced major axis (RMA) regression (Meek et al., 1998).

The statistical analysis of the NOAA IRGA was nearly identical to the second analysis of the LI-7500. The notable differences were that S^{out} was not measured. Without a thermocouple measurement of S^{out}, the sonic anemometer S^{sonic} was used to calculate two versions of ΔS_{EC}: one as S^{path} - S^{sonic} and the other as $S^{path,TCAdj}$ - S^{sonic} where the same thermocouple adjustment was applied as described above. Thus, we conducted four weighting analyses: (1) predicting $\Delta S_{EC} = S^{path}$ - S^{sonic} from $\hat{S}^{bot}$, $\hat{S}^{top,NOAA}$, and S^{spar} and obtaining the posterior derived quantity $\Delta S^{surf,NOAA}(\hat{\delta}, \omega_{posterior})$, (2) predicting $\Delta S_{EC} = S^{path}$ - S^{sonic} with the Bayesian cut function applied to ω^{spar}, (3) predicting $\Delta S_{EC} = S^{path,TCAdj}$ - S^{sonic} and obtaining the posterior derived quantity $\Delta S^{surf,NOAA}(\hat{\delta}, \omega_{posterior})$, and (4) predicting $\Delta S_{EC} = S^{path,TCAdj}$ - S^{sonic} with the Bayesian cut function applied to ω^{spar}.

We performed all statistical analyses using R (version 3.5.1), (R Core Team, 2015) within RStudio (version 1.1.456), (RStudio Team, 2015), using packages CODA (Plummer et al., 2006) and rjags (Plummer, 2015b) with the MCMC analysis implemented by JAGS (version 4.0.0), (Plummer, 2003). In the weighting analyses the Bayesian cut function was applied to the S^{path}, S^{out}, S^{bot}, S^{top}, and S^{spar} parameters (i.e. the uncertainty in the different S values is influenced by the uncertainty in the thermocouple measurements but not in the uncertainty of the weightings). We use embarrassingly parallel MCMC techniques (Neiswanger et al., 2014; Rosenthal, 2000; Wilkinson, 2006) to implement the Bayesian cut function (Plummer, 2011) and to improve convergence. This means that instead of running N steps in a single MCMC chain, N MCMC chains are run for only a few steps and then combined. In all instances, 1000 embarrassingly parallel analyses were combined, each one with 1000 MCMC steps of burn-in, and then combining the final values of each process parameter to form posterior distributions. We make statistical inferences by comparing the 95% credible intervals of the posterior distributions and derived quantities (Lu et al., 2012). We report the efficiency of a model (R^2), which is calculated as $1\text{-}\Sigma(\Delta S_{EC}\text{-}\Delta S^{surf})^2/\Sigma(\Delta S_{EC}\text{-}\overline{\Delta S}_{EC})^2$ where $\overline{\Delta S}_{EC}$ is the mean of ΔS_{EC} (Nash and Sutcliffe, 1970). Except for analyses using $\omega_{posterior}$, ΔS^{surf} is not derived from a statistical fit of ΔS_{EC}, hence R^2 values based on the residual difference between the two estimates of the IRGA self-heating term can be negative, which indicates the modeled self-heating correction is less accurate than a simple average (Vanclay and Skovsgaard, 1997). We do not report the posterior process parameters for random effects.

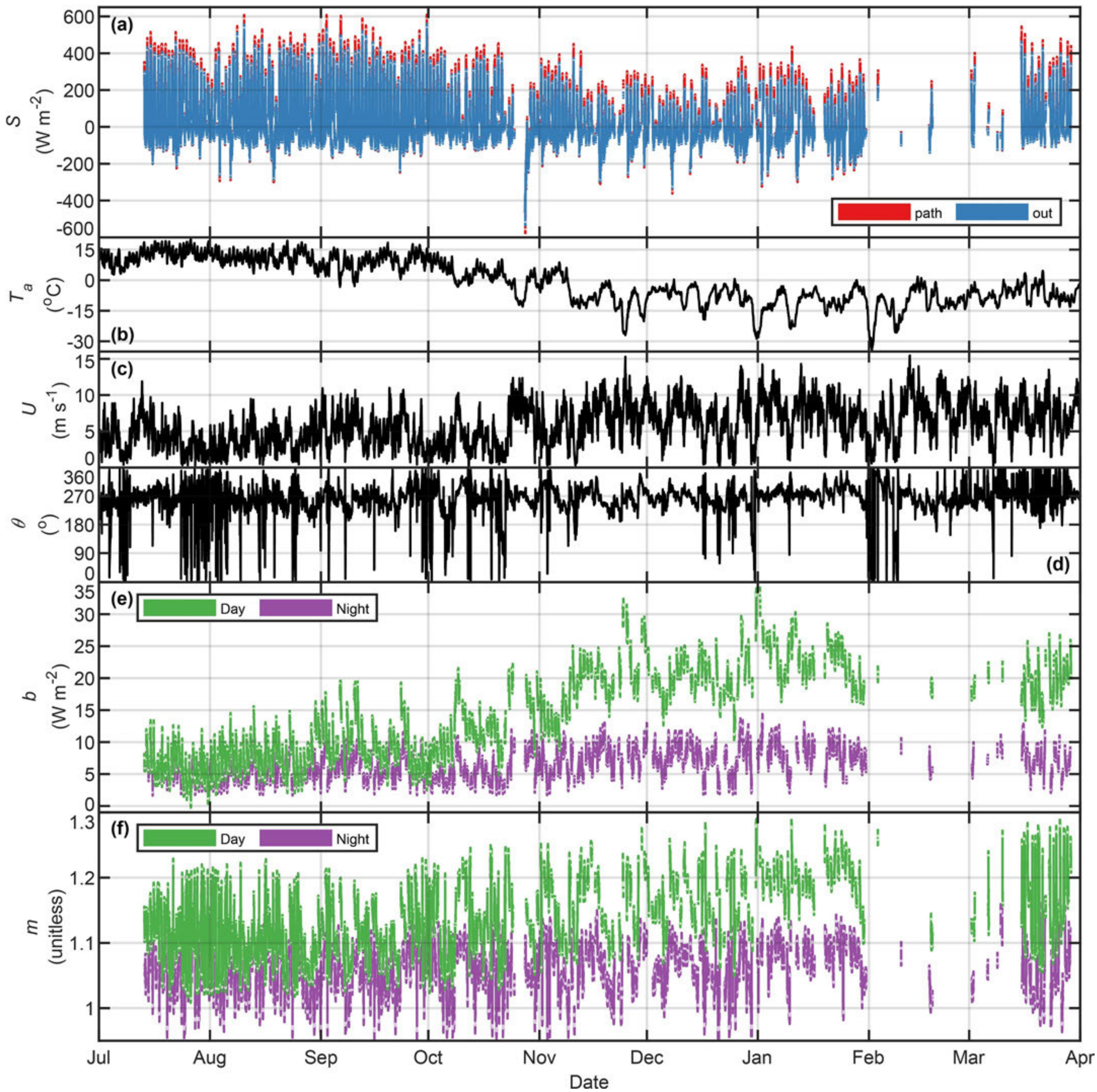

Fig. 3. (a) Sensible heat flux measured via eddy covariance using thermocouples inside (S^{path}, red shading) and outside (S^{out}, blue shading) of the LI-7500 path. Environmental covariates (b) ambient temperature (T_a), (c) wind speed (U), and (d) wind direction (θ) used in the statistical analysis. Bayesian (e) offset and (f) slope parameters testing for additional sensible heat flux within the LI-7500 path during the day (green shading) and night (purple shading). Shading (i.e. light/dark) represents the median, inner quartile range, and 95% credible interval of the posterior distribution for each process parameter and derived quantity.

3. Results

The LI-7500 study resulted in 9,202 half-hours of complete data from all fifteen thermocouples from July 2010 to March 2011 (Fig. 3). The Bayesian statistical analysis confirmed significant additional sensible heat flux within the path of the IRGA. The offset parameter was significantly greater than 0 W m^{-2} during the entire study, with significantly more heating during the day and from October through May (Fig. 3e). The slope parameter was significantly greater than 1 during the day throughout the entire study and it also increased during the winter (Fig. 3f), though this was less pronounced than with the offset parameter. The parameters associated with ambient temperature were negative (i.e., the self-heating offset and slope increased with lower temperatures), wind speed were positive (i.e., the self-heating offset and slope increased with higher winds), and wind direction were positive (i.e., with the IRGA tilted north, winds out of the north increased the self-heating offset and slope and winds from the south decreased them) (Table 1). The positive increase in slope associated with wind direction at night means that while sensible heat fluxes are typically negative, the sensible heat flux within the path tends be more negative for winds blowing into the analyzer. Overall, the sensible heat flux within the path is higher than ambient air at night, but this is associated

Table 1
Bayesian offset and slope parameters testing for additional sensible heat flux in the LI-7500 path by comparing eddy covariance measurements using thermocouples inside and outside (S^{path} and S^{out}) of the IRGA path. Environmental covariates (day/night, ambient temperature, wind speed, and wind direction) were chosen via model selection analysis and normalized. The Bayesian posterior parameters are summarized as median (95% Bayesian credible interval); random effect parameters are not reported.

Environmental covariates		Offset parameter (W m^{-2})	Slope parameter (unitless)
-	Day	11.7 (10.6–12.8)	1.146 (1.135–1.158)
	Night	2.4 (1.6–3.2)	1.037 (1.019–1.056)
Ambient temperature	Day	-5.3 (-5.8 to -4.8)	-0.021 (-0.026 to -0.017)
	Night	-	-
Wind speed	Day	1.9 (1.5–2.4)	0.005 (0.000–0.010)
	Night	2.0 (1.6–2.5)	0.013 (0.005–0.020)
Wind direction	Day	1.1 (0.2–1.9)	0.089 (0.080–0.097)
	Night	-	0.067 (0.055–0.078)

with the more dominant effects such as temperature and wind speed (Table 1).

During the LI-7500 study, winds with a median velocity of $U = 4.2$ m s^{-1} led to boundary layers with median thicknesses of $\delta_{B08}^{bot,LI7500} = 4.5$ mm, $\delta_{B08}^{top,LI7500} = 4.8$ mm, and $\delta^{spar} = 0.20$ mm; results for the new formulation were $\hat{\delta}^{bot} = 0.50$ mm and $\hat{\delta}^{top,LI7500} = 0.35$ mm. Temperatures were generally higher than ambient on all surfaces, with the bottom being warmest and the spar being warmer than the top (Fig. 4a). The median temperature gradients were $\Delta T^{bot} = 1.4$°C, $\Delta T^{top} = 0.0$°C, and $\Delta T^{spar} = 0.3$°C. The B08 formulation had noticeably small top and bottom surface heat fluxes (Fig. 4c, e) which had medians of $S_{B08}^{bot,LI7500} = 7$ W m^{-2}, $S_{B08}^{top,LI7500} = 0$ W m^{-2}, and $S^{spar} = 32$ W m^{-2}. The top and bottom surface heat fluxes in the new formulation had more similar magnitudes to the spar (Fig. 5a-c) with medians of $\hat{S}^{bot} = 68$ W m^{-2} and $\hat{S}^{top,LI7500} = 0$ W m^{-2}.

The LI-7500 self-heating was measured via eddy covariance with thermocouples inside and outside of the IRGA path (Figs. 3a, 4f, 5d). In addition, it was estimated by different weighted sums of the surface heat fluxes. Combining surface heat fluxes based on the δ_{B08} boundary layers with the ω_{B08} a priori weightings resulted in ΔS^{surf} that were reasonably similar to ΔS_{EC} (Fig. 4f); under these conditions the weightings in Eq. 3 were plausible, especially for ω_{B08}^{bot} and ω_{B08}^{spar} (green dot, Fig. 6). Likewise, combining surface heat fluxes based on the $\hat{\delta}$ boundary layers with the $\hat{\omega}^{LI7500}$ a priori weightings resulted in ΔS^{surf} that were also similar to ΔS_{EC} (Fig. 5d); the weighting analyses also indicated that the weightings in Eq. 14 were plausible (purple dot, Fig. 7). We considered other combinations, such that with the δ_{B08} boundary layers the $\hat{\omega}^{LI7500}$ a priori weightings were plausible (purple dot, Fig. 6) while with the $\hat{\delta}$ boundary layers with the ω_{B08} a priori weightings were not (green dot, Fig. 7).

ΔS from the sum of the LI-7500 surface heat fluxes were similar to ΔS from eddy covariance measurements for all but one combination of boundary layers and weightings. For ΔS_{EC} the mean ± standard deviation was 19.2 ± 29.8 W m^{-2} (Table 2). Estimates of ΔS^{surf}, except for $\Delta S^{surf,LI7500}(\hat{\delta}, \omega_{B08})$ and $\Delta S^{surf,LI7500}(\delta_{B08}, \hat{\omega})$, had means between 16.6-20.1 W m^{-2}, standard deviations between 20.5-25.1 W m^{-2} (Table 2), and generally fit the ΔS_{EC} data (Fig. 8a, d-f) with R^2 values between 0.62-0.66. $\Delta S^{surf,LI7500}(\delta_{B08}, \hat{\omega})$ was also correlated with ΔS_{EC} (Fig. 8c, $R^2 = 0.62$) but estimated a smaller magnitude for self-heating (Table 2, 13.1 ± 19.9 W m^{-2}). The major exception was $\Delta S^{surf,LI7500}(\hat{\delta}, \omega_{B08})$ with $\hat{\delta}$ from this study and ω_{B08} from Burba et al. (2008), which had mean ± standard deviation of 84.6 ± 95.4 W m^{-2} (Table 2) and did not fit the ΔS_{EC} data (Figure 8b, $R^2 = -13.74$).

The NOAA IRGA study resulted in 4694 half-hours of complete data from all twelve thermocouples from February to June 2010. During this study, winds with a median velocity of $U = 3.4$ m s^{-1} led to boundary layers with median thicknesses of $\hat{\delta}^{bot} = 0.65$ mm, $\hat{\delta}^{top,NOAA} = 0.61$ mm, and $\delta^{spar} = 0.31$ mm. The median temperature gradients were $\Delta T^{bot} = 4.4$°C, $\Delta T^{top} = 0.4$°C, and $\Delta T^{spar} = 1.4$°C. The resulting surface heat fluxes (Fig. 9d-f) had medians of $\hat{S}^{bot} = 154$ W m^{-2}, $\hat{S}^{top,LI7500} = 15$ W m^{-2}, and $S^{spar} = 107$ W m^{-2}.

The sensible heat flux within the NOAA IRGA path was measured via eddy covariance with thermocouples (Fig. 9a, green shading) and ΔS_{EC} was determined relative to the sonic anemometer (Fig. 9a, black line) with adjustments made for the thermocouple time constant (Fig. 9g, green and purple shading). In addition, ΔS^{surf} was estimated by different weighted sums of the surface heat fluxes. The ω_{B08}^{bot}, ω_{B08}^{top}, and $\hat{\omega}^{spar,NOAA}$ a priori weightings (i.e. similar to Burba et al. (2008)) resulted in $\Delta S^{surf,NOAA}(\hat{\delta}, \omega_{B08}, \hat{\omega})$ that were not similar to ΔS_{EC} (Fig. 9g, brown shading) while $\Delta \hat{S}^{surf,NOAA}$ based on the $\hat{\omega}^{NOAA}$ weightings was similar (Fig. 9g, pink shading). Bayesian analyses of the surface heat flux weightings indicated that the weightings in Eq. 20 are not plausible, regardless of whether or not the thermocouple adjustment was included in ΔS_{EC} (Figs. 10–11, green dots.); the weighting in Eq. 19 were plausible (Fig. 10–11, purple dots).

For the NOAA IRGA, ΔS_{EC} measurements were similar to ΔS^{surf} estimates, except for one case. For ΔS_{EC}, the mean ± standard deviation was 39.3 ± 36.7 W m^{-2}, which increased to 57.1 ± 48.8 W m^{-2} when the thermocouple adjustment was applied (Table 3). For all but the weighting that featured ω_{B08}, ΔS^{surf} had means between 38.1-56.9 W m^{-2} and standard deviations between 13.1-28.0 W m^{-2} (Table 3), and generally fit the ΔS_{EC} and $\Delta S_{EC,TC\ Adj}$ data (Figure 12c-f) with R^2 values between -0.30 to -0.07 when compared to ΔS_{EC} and between 0.38-0.50 when compared to $\Delta S_{EC,TC\ Adj}$. In the case of the ω_{B08}^{bot}, ω_{B08}^{top}, and $\hat{\omega}^{spar,NOAA}$ weighting, $\Delta S^{surf,NOAA}(\hat{\delta}, \omega_{B08}, \hat{\omega})$ had mean ± standard deviation of 217.4 ± 94.7 W m^{-2} (Table 3) and did not fit the ΔS_{EC} or $\Delta S_{EC,TC\ Adj}$ the data (Fig. 12a-b, R^2 values of -43.68 and -16.61).

4. Discussion

The results from our field studies indicate that IRGA self-heating in a cold, windy, high elevation, mountainous field site is evident and pronounced during daytime and wintertime; therefore we retain our hypothesis (1). While self-heating can be reasonably estimated from the weighted sum of surface heat fluxes, we find inconsistences with the Burba et al. (2008) correction. We determine that both the bottom and top boundary layers in B08 have unwarranted constants the lead to surface heat fluxes that are about an order of magnitude less than what should be expected; therefore we retain our hypothesis (2). We also determine that the sum of surface heat fluxes in B08 weights the heat fluxes from bottom and top surfaces are improbable, and are about an order of magnitude too large. At our field site, these errors approximately cancel out and lead to the reasonable estimates of the IRGA self-heating. Finally, we find that a weighted sum based on the proportion of surface area contributed to the measurement volume provides reasonable estimates of the IRGA self-heating; therefore we retain our hypothesis (3).

4.1. Interpreting self-heating from the NOAA IRGA

Though the NOAA IRGA is seldom used today, it was a precursor of the LI-7500 for open-path eddy covariance measurements (Auble and Meyers, 1992). Investigations of IRGA self-heating for this sensor are rare, with one example being Ikawa et al. (2013) who applied the Burba et al. (2008) LI-7500 correction while acknowledging that the “appropriate correction … is probably different”. As pictured in Fig. 2, the NOAA IRGA has a similar general shape as the LI-7500, but with one distinct and important difference: the top and bottom surfaces are

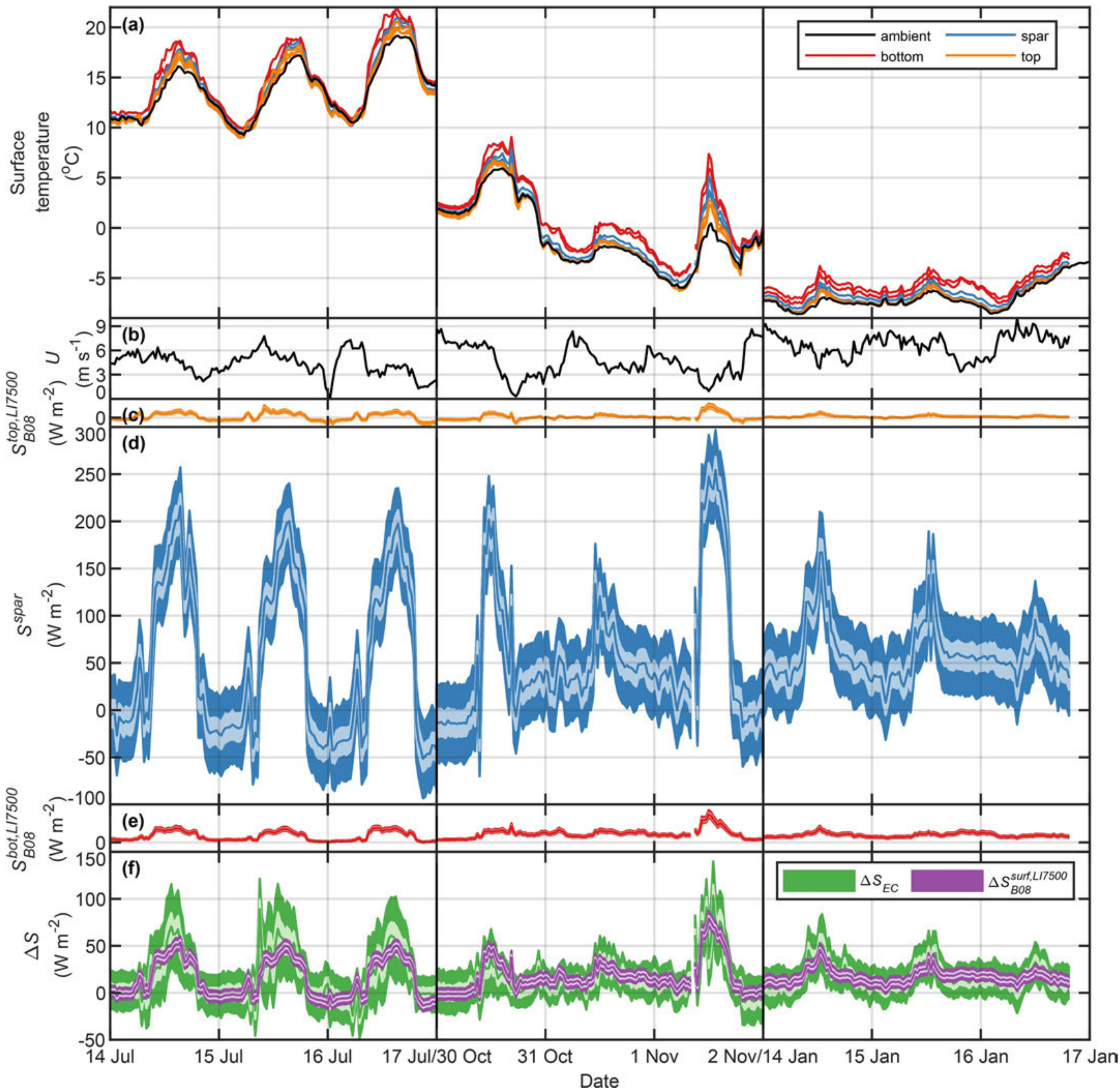

Fig. 4. An illustration from this study of the LI-7500 self-heating correction as defined by Burba et al. (2008). (a) Ambient and LI-7500 surface temperatures are combined with (b) wind speed (U) to estimate the surface heat fluxes (c) $S_{B08}^{top,LI7500}$, (d) S^{spar}, and (e) $S_{B08}^{bot,LI7500}$. (f) The additional heat flux inside the LI-7500 path, ΔS, was measured via eddy covariance (EC) using thermocouples inside and outside of the IRGA path (green shading); ΔS was also estimated from Eq. 3 with a weighted sum of heat fluxes from key instrument surfaces ($\Delta S_{B08}^{surf,LI7500}$, purple shading). Shading (i.e. light/dark) represents the median, inner quartile range, and 95% credible interval of the posterior distribution for each process parameter and derived quantity. The ΔS_{EC} is thermocouple adjusted such that S^{out} has the same magnitude as the sonic anemometer S^{sonic}. Panels c-f have the same vertical scaling.

flat. This is key, because it invalidates the 4 mm and 4.5 mm boundary layer adjustment terms for non-flat surfaces in Eqs. 5 and 7 of the B08 correction; of a minor importance is that the definition of $\hat{\delta}^{top,NOAA}$ should be based on the Nobel (1983) formulation for a flat surface instead of a sphere. Thus, keeping with the general principles of Nobel (1983), the only justifiable boundary layers for the bottom, top, and spar are Eqs. 9–10, 17, leading to $\delta^{bot,NOAA}$ and $\delta^{top,NOAA}$ being ~0.6 mm.

The ramifications of this become clearer when evaluating the weighted sum of the surface heat fluxes. As Ikawa et al. (2013) acknowledged, the NOAA IRGA correction is probably different, and the value of $\omega_{B08}^{spar,LI7500} = 0.15$ in Eq. 3 is dubious for the NOAA IRGA; instead we propose the value 0.261 derived from the surface area of the measurement volume exposed to the spar. Of more importance is a test of the validity of $\omega_{B08}^{bot} = \omega_{B08}^{top} = 1$. Based on the results in Figs. 9g (brown shading), 10-11 (green versus blue dots), and 12a-b and Table 3 ($\Delta S^{surf,NOAA}(\hat{\delta}, \omega_{B08}, \hat{\omega})$ with mean ± standard deviation of 217.4 ± 94.7 W m^{-2} versus ΔS_{EC} and $\Delta S_{EC,TC\ adj}$ with mean ± standard deviation of 39.3 ± 36.7 W m^{-2} and 57.1 ± 48.8 W m^{-2}, respectively), we reject this assumption.

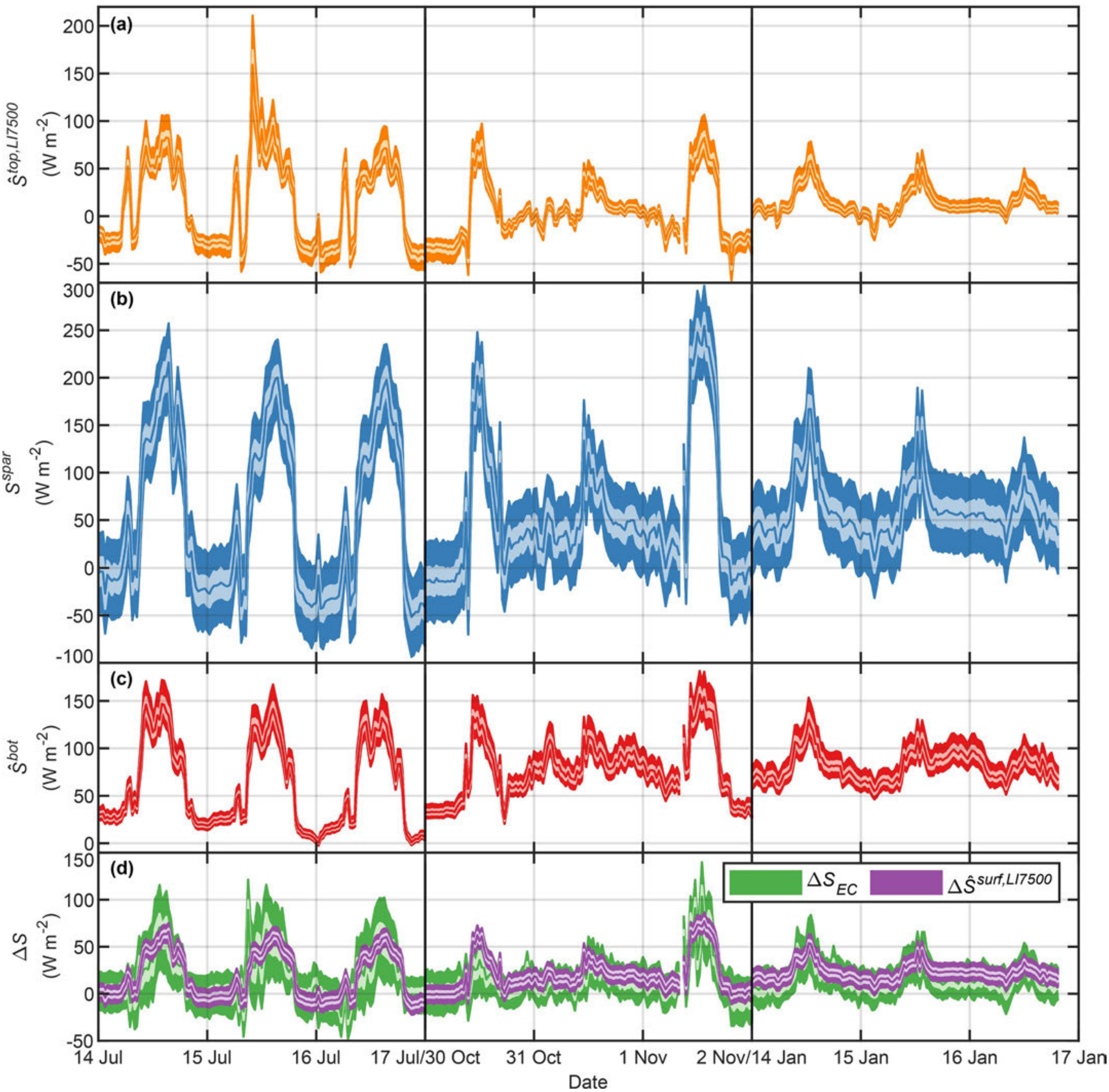

Fig. 5. The same as Fig. 4, except illustrating the LI-7500 self-heating correction as defined by this study. The data in Fig. 4a-b are used to estimate the surface heat fluxes (a) $\hat{S}^{top,LI7500}$, (b) S^{spar} (which is identical to Fig. 4d), and (c) $\hat{S}^{bot}$. (d) The additional heat flux, ΔS, was measured via eddy covariance (EC, green shading) and estimated from Eq. 14 with a weighted sum of heat fluxes from key instrument surfaces ($\Delta\hat{S}^{surf,LI7500}$, purple shading). Shading (i.e. light/dark) represents the median, inner quartile range, and 95% credible interval of the posterior distribution for each process parameter and derived quantity. The ΔS_{EC} is thermocouple adjusted such that S^{out} has the same magnitude as the sonic anemometer S^{sonic}.

Instead, in this study we propose a weighted sum proportional to the amount of area each heated surface contributes to the measurement path. For the NOAA IRGA, this leads to Eq. 19, which based on the results in Figs. 9g (pink shading), 10-11 (purple versus blue dots), and 12c-d and Table 3 ($\Delta\hat{S}^{surf,NOAA}$ with mean ± standard deviation of 45.0 ± 21.9 W m^{-2}), we retain our hypothesis. This is further supported by the Bayesian posterior weightings in Fig. 12e-f and Table 3 (ΔS^{surf} from the posterior fits with mean ± standard deviation of 38.1 ± 13.1 W m^{-2} and 28.0 W m^{-2}). Compared to $\Delta S_{EC,\ TC\ adj}$, the a priori weightings of $\hat{\omega}^{bot,NOAA} = \hat{\omega}^{top,NOAA} = 0.069$ were probable (Figs. 11, purple versus red dots, Table 3 credible intervals for the posteriors of ω^{bot} and ω^{top} contain 0.069); the comparison to the non-adjusted ΔS_{EC} indicates the a prior weightings were plausible but improbable (Figs. 10, purple versus blue dots).

The major concept in the new formulation's definitions of $\hat{\omega}$ is that contribution of the bottom and top surfaces should take into account the size of these heating surfaces relative to the volume of the air parcel in the path of the IRGA. This intuitively makes sense if an IRGA were designed with an arbitrarily long path length; as the path length approaches infinity, the contribution of the bottom and the top surfaces

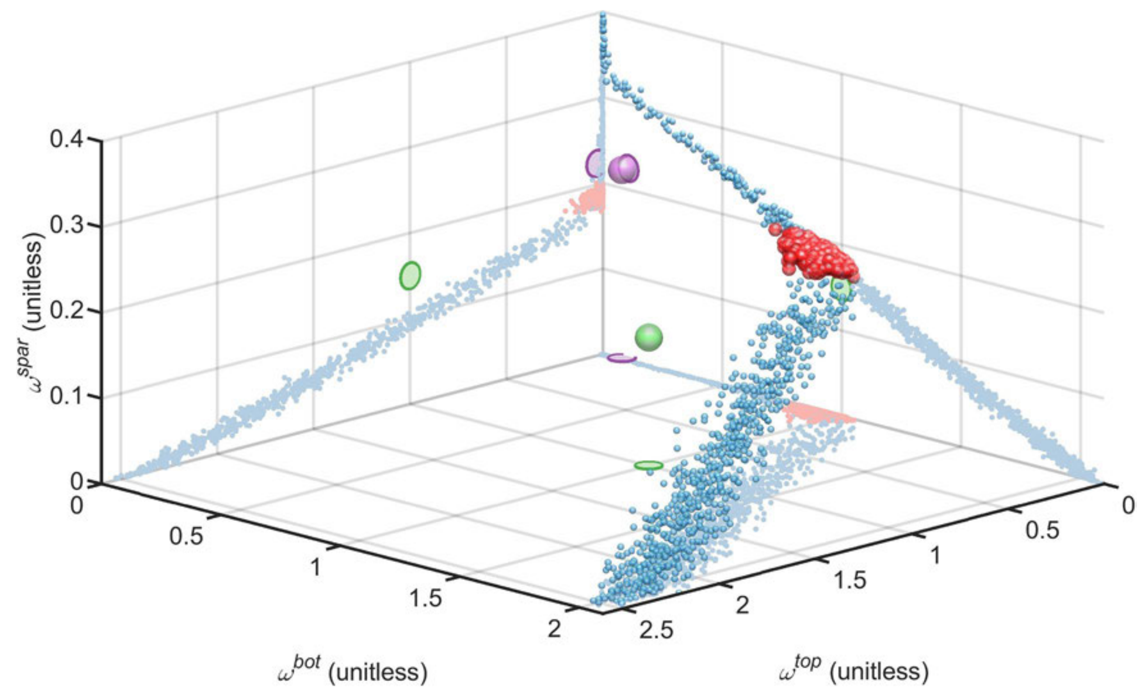

Fig. 6. Bayesian analysis of the weighted sum of surface heat fluxes defined by Burba et al. (2008) (i.e., $S_{B08}^{bot,LI7500}$, $S_{B08}^{top,LI7500}$, and S^{spar}) required to match the LI-7500 self-heating measured with eddy covariance. The green dot is the a priori weighting defined by Burba et al. (2008) with parameters ω_{B08}^{bot}, ω_{B08}^{top}, and ω_{B08}^{spar} from Eq. 3; these values were used to define the prior probability distributions in the Bayesian analyses. The purple dot is the a priori weighting defined by this study with parameters $\hat{\omega}^{bot,LI7500}$, $\hat{\omega}^{top,LI7500}$, and $\hat{\omega}^{spar,LI7500}$ from Eq. 14. The blue dots are plausible Bayesian posterior weightings obtained by applying the Bayesian cut function to the ω^{spar} parameter; the red dots are obtained without the Bayesian cut function.

should become negligible. While this might seem unrealistic, instruments such as the LI-7700 open-path methane analyzer have a single path length ~4 times longer than the LI-7500 while laser absorption spectrometers can utilize multiple reflections to create path lengths of ~80 m (Ono et al., 2014). Another consequence of defining $\hat{\omega}$ in this manner is that the contribution of the spar is emphasized, especially for longer path lengths. In the case of an infinitely long NOAA IRGA the spar would be able to deliver heat to 30% of the surface area of the measurement volume; for the LI-7500 this number approaches 26%. While we can reject the hypothesis that $\omega^{bot} = \omega^{top} = 1$, we cannot reject the concept of defining $\hat{\omega}$ based on the proportion of surface area that contributes sensible heat flux to the path. Because of the structural resemblance between the NOAA IRGA and the LI-7500 (Figs. 1-2), we conclude that this applies for both sensors.

4.2. Interpreting self-heating from the LI-7500

The results from the LI-7500 study demonstrate that accurate self-heating estimates require appropriate pairings of surface boundary layer definitions and surface heat flux weightings. The combinations of δ_{B08} and ω_{B08} (Fig. 4f, purple shading; Fig. 8a; and Table 2, $\Delta S_{B08}^{surf,LI7500}$ with mean ± standard deviation of 16.6 ± 21.3 W m^{-2} versus ΔS_{EC} with mean ± standard deviation of 19.2 ± 29.8 W m^{-2}) and $\hat{\delta}$ and $\hat{\omega}^{LI7500}$ (Fig. 5d, purple shading; Fig. 8d; Table 2, $\Delta \hat{S}^{surf,LI7500}$ with mean ± standard deviation of 20.1 ± 25.1 W m^{-2}) both resulted in accurate self-heating estimates. The weighting analyses reaffirmed that these combinations were plausible (Fig. 6, green versus blue dots; Fig. 7, purple versus red dots; Fig. 8e-f) and the posterior weightings were similar to ω_{B08} (for $\Delta S^{surf,\ LI7500}(\delta_{B08}, \omega_{posterior})$ the ω^{bot} credible interval includes 1 while ω^{spar} lower credible limit is 0.176) and $\hat{\omega}^{LI7500}$ (for $\Delta S^{surf,LI7500}(\hat{\delta}, \omega_{posterior})$ the ω^{bot} lower credible limit is 0.111 and ω^{top} credible interval includes 0.035). It merits consideration that the only non-informative Bayesian prior probability distributions in this study where for the weightings, which had expected values of $\omega^{bot} = \omega^{top} = 1$ and $\omega^{spar,LI\text{-}7500} = 0.15$. In contrast, the poor results from the combination of $\hat{\delta}$ with ω_{B08} (Fig. 7, green versus blue dots; Fig. 8b; Table 2, $\Delta S^{surf,LI7500}(\hat{\delta}, \omega_{B08})$ with mean ± standard deviation of 84.6 ± 95.4 W m^{-2}) lead us conclude that if the boundary layer adjustment terms for non-flat surfaces are unwarranted, then the weightings of B08 are not possible.

While it is possible that the δ_{B08} boundary layers could be valid even if the ω_{B08} weightings are rejected (Fig. 8c; Table 2, $\Delta S^{surf,LI7500}(\delta_{B08}, \hat{\omega})$ with mean ± standard deviation of 13.1 ± 19.9 W m^{-2}; R^2 = 0.62), there are reasons to consider this unlikely. First, the combination of δ_{B08} with $\hat{\omega}^{LI7500}$ is improbable (Fig. 6, purple versus red dots; Table 2, ω^{bot} lower credible limit is 0.820 versus $\hat{\omega}^{bot,LI7500} = 0.108$). Second, the magnitude of $\Delta S^{surf,LI7500}(\delta_{B08}, \hat{\omega})$ is ~1/3 smaller than ΔS_{EC} (Table 2). Third, essentially all of the self-heating is attributed to the spar (Table 2, mean ± standard deviation of 12.2 ± 19.2 W m^{-2} for the spar versus means and standard deviations between 0.0 and 0.9 W m^{-2} for the bottom and top). These results are based on $\hat{\omega}^{spar,LI7500} = 0.225$; had the value $\omega_{B08}^{spar,LI7500} = 0.15$ been used it is doubtful that the boundary layers δ_{B08} could be considered possible. Conversely, to increase the magnitude of ΔS^{surf} to match ΔS_{EC} then $\omega^{spar,LI\text{-}7500}$ would need to be even larger, i.e. ~0.3 (Fig. 6, closest blue dots near purple dot), which is difficult to justify from first principles. Because we believe the results of the NOAA IRGA study invalidate the B08 weightings, we contend that the consequences of accepting the B08 boundary layer definitions is to accept that the self-heating contribution from the bottom and top surfaces is negligible. We find this conclusion dubious, considering the bottom surface of the LI-7500 was consistently the warmest (Fig. 4a, red lines). For the NOAA IRGA, the bottom surface was also the warmest (Fig. 9b, red lines) while the estimated surface heat flux was a similar magnitude to that of the spar (Fig. 9e-f); it is reasonable to expect that the LI-7500 operates in a similar manner. There are other reasons to suspect that the δ_{B08} boundary layers are invalid. First, the underlying basis for the 4 mm and 4.5 mm boundary layer adjustment terms in Eqs. 5 and 7 is that the curvature of these

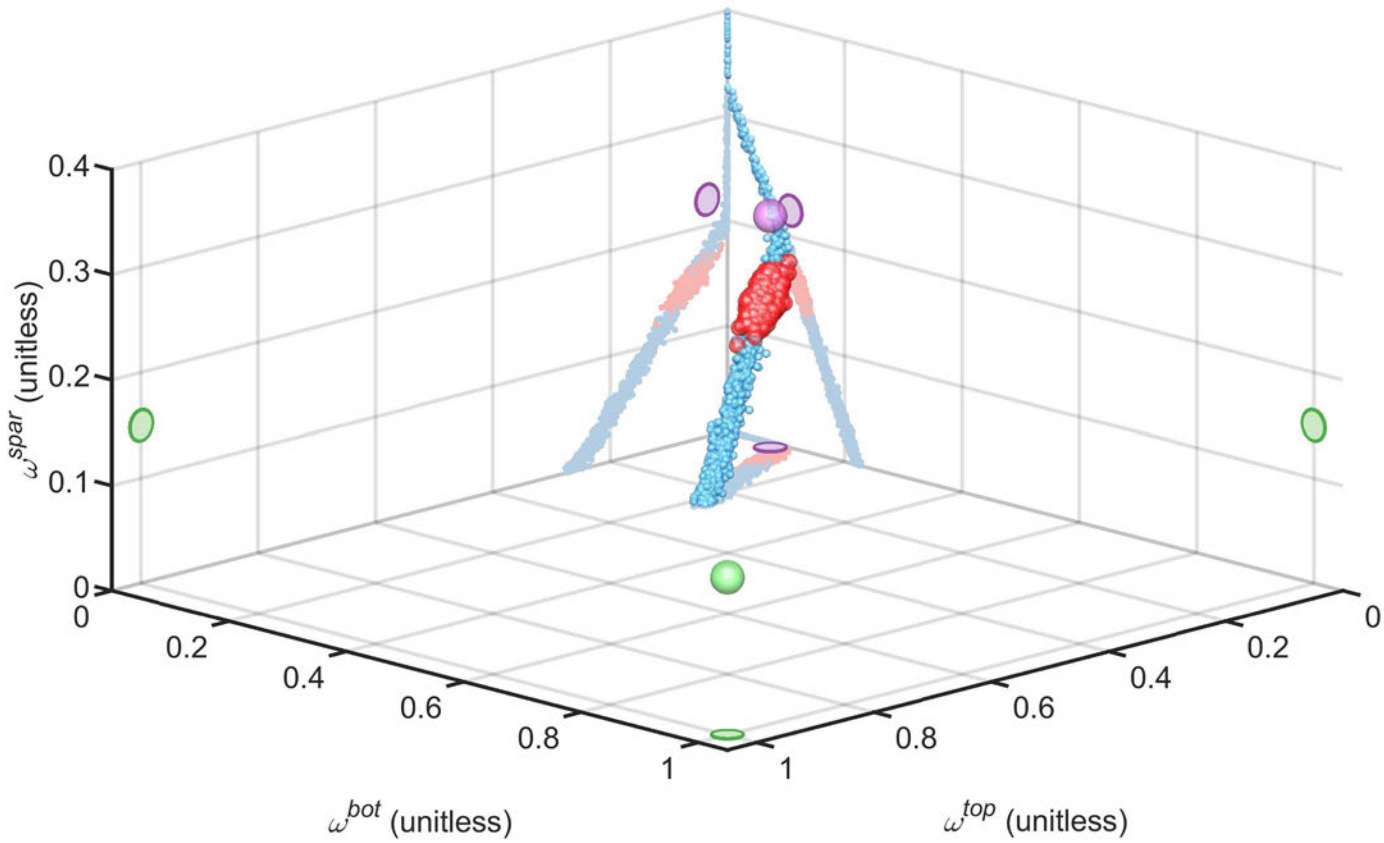

Fig. 7. Bayesian analysis of the weighted sum of surface heat fluxes defined by this study (i.e., $\hat{S}^{bot}$, $\hat{S}^{top}_{LI7500}$, and S^{spar}) required to match the LI-7500 self-heating measured with eddy covariance. The green dot is the a priori weighting defined by Burba et al. (2008) with parameters ω^{bot}_{B08}, ω^{top}_{B08}, and $\omega^{spar,LI7500}_{B08}$ from Eq. 3; these values were used to define the prior probability distributions in the Bayesian analyses. The purple dot is the a priori weighting defined by this study with parameters $\hat{\omega}^{bot,LI7500}$, $\hat{\omega}^{top,LI7500}$, and $\hat{\omega}^{spar,LI7500}$ from Eq. 14. The blue dots are plausible Bayesian posterior weightings obtained by applying the Bayesian cut function to ω^{spar}; the red dots are obtained without the Bayesian cut function.

surfaces would lead to air pockets that mix poorly. This assumption might be dubious, especially at turbulent sites such as GLEES (Frank et al., 2014). Second, if the bottom was conceptualized as a purely round object (an assumption that could apply in the vicinity of the bottom window) then using the Nobel (1983) formulation for a sphere with a diameter of $l = 0.118$ (the LI-7500 base height) or $l = 0.087$ m (i.e., the geometric mean of the height and dimeter of the LI-7500 base) the resulting median δ^{bot} values would be between 0.46-0.53 mm; these are clearly in contradiction to the 4 mm and 4.5 mm constants in Eqs. 5 and 7. Based on these considerations, we believe that the boundary layer adjustment terms for non-flat surfaces in B08 are unwarranted.

Though we focus on the upper surface of the bottom of the IRGA, the potential for heat to be contributed from the sides of the cylindrical object should also be considered. Convection can create boundary layers with strong upward flow around the sides of heated vertical

Table 2

The additional heat flux, ΔS, in the LI-7500 path measured via eddy covariance (EC) using thermocouples inside and outside (S^{path} and S^{out}) of the IRGA path versus estimated with a weighted (ω^{bot}, ω^{top}, and ω^{spar}) sum of heat fluxes from key instrument surfaces (S^{bot}, S^{top}, and S^{spar}). Two sets of surface boundary layer equations (δ_{B08} from Burba et al. (2008) and $\hat{\delta}$ from this study) were used to calculate surface heat fluxes and four weightings were implemented (ω_{B08} a priori from Burba et al. (2008), $\hat{\omega}^{LI7500}$ a priori from this study, and the Bayesian posteriors that predict ΔS_{EC} from the surface heat fluxes based on δ_{B08} and $\hat{\delta}$). The Bayesian posterior weighting parameters are summarized as median (95% Bayesian credible interval); random effect parameters are not reported. The derived quantities for ΔS and the surface heat fluxes have posterior distributions which are summarized as mean ± standard deviation. ΔS_{EC} is thermocouple adjusted such that S^{out} has the same magnitude as the sonic anemometer S^{sonic}.

Measurement	Surface boundary layer	Surface heat flux weighting	ω^{bot} (unitless)	ω^{top} (unitless)	ω^{spar} (unitless)	$\omega^{bot}S^{bot}$ (W m^{-2})	$\omega^{top}S^{top}$ (W m^{-2})	$\omega^{spar}S^{spar}$ (W m^{-2})	ΔS (W m^{-2})
EC	-	-	-	-	-	-	-	-	19.2 ± 29.8
IRGA surface temperature	δ_{B08}	ω_{B08}	1	1	0.15	8.2 ± 5.7	0.3 ± 3.9	8.1 ± 12.8	16.6 ± 21.3
		$\hat{\omega}^{LI7500}$	0.108	0.035	0.225	0.9 ± 0.6	0.0 ± 0.1	12.2 ± 19.2	13.1 ± 19.9
		$\omega_{posterior}$	0.919 (0.820–1.012)	0.017 (0.001–0.093)	0.187 (0.176–0.197)	7.5 ± 5.2	0.0 ± 0.1	10.1 ± 16.0	17.6 ± 20.5
	$\hat{\delta}$	ω_{B08}	1	1	0.15	71.3 ± 47.9	5.1 ± 39.4	8.1 ± 12.8	84.6 ± 95.4
		$\hat{\omega}^{LI7500}$	0.108	0.035	0.225	7.7 ± 5.2	0.2 ± 1.4	12.2 ± 19.2	20.1 ± 25.1
		$\omega_{posterior}$	0.125 (0.111–0.139)	0.062 (0.034–0.094)	0.150 (0.132–0.169)	8.9 ± 6.0	0.3 ± 2.5	8.1 ± 12.8	17.4 ± 20.5

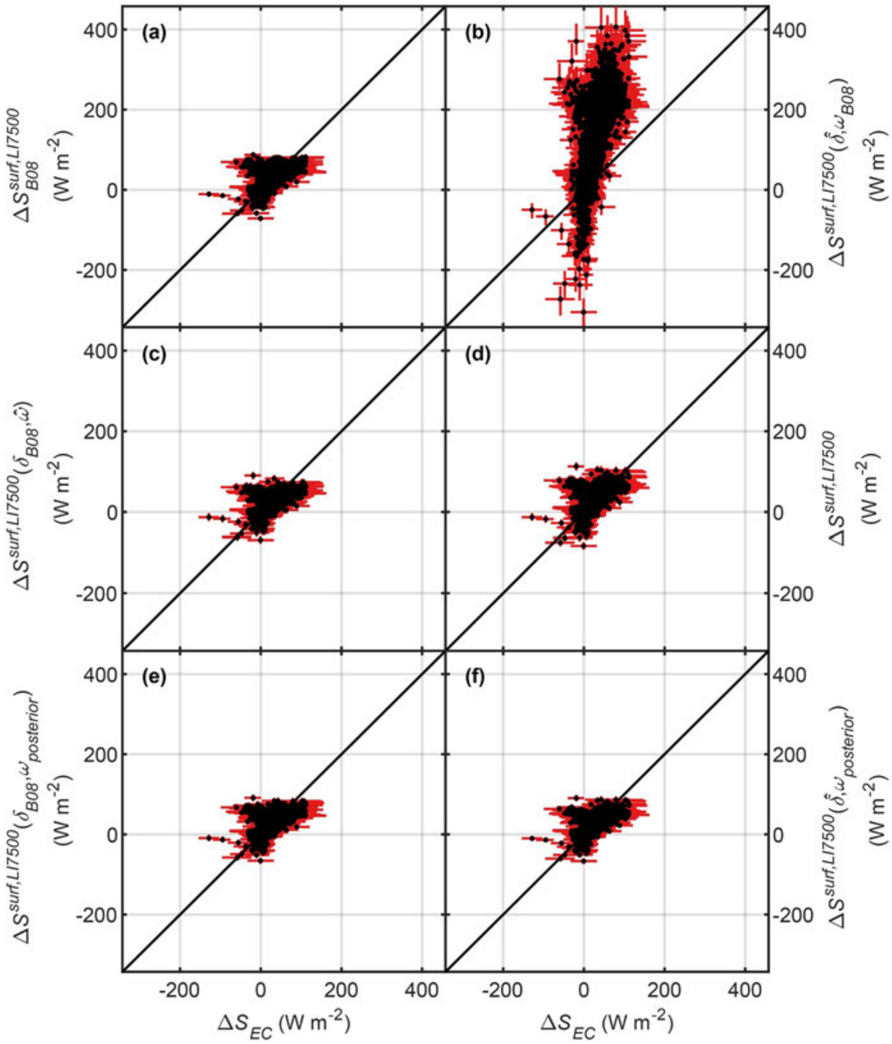

Fig. 8. Comparisons of the additional heat flux in the LI-7500 path, ΔS, for each half-hour measured via eddy covariance (EC) using thermocouples inside and outside of the IRGA path versus estimated with a weighted sum of heat fluxes from key instrument surfaces (ΔS^{surf}). (a, c, e) The δ_{B08} surface boundary layers are from Burba et al. (2008) and in (b, e, f) they are $\hat{\delta}$ from this study. The weighting parameters in (a-b) are ω_{B08} defined a priori from Burba et al. (2008) (Eq. 3), in (c-d) are $\hat{\omega}^{LI7500}$ defined a priori from this study (Eq. 14), and in (e-f) are the Bayesian posterior weightings that most likely predict ΔS_{EC}. The red shading represents the 95% credible interval of the posterior distribution for each derived quantity.

cylinders (Goodrich and Marcum, 2019) which can increase the temperature and wind velocity well above the upper surface (Senapati et al., 2017). Though this effect is difficult to quantify, the revised self-heating correction may adequately account for it. First, without independent measurements, the side of the cylinder can be assumed to have a temperature similar to T_s^{bot}. Second, the boundary layers that form on the sides of the cylinder are likely to be similar to $\hat{\delta}^{bot}$, as demonstrated by the differences between Eqs. 9 and 10 for cylinders and flat surfaces. Taken together, the heat flux from the side of the cylinder should be of a similar shape and magnitude to $\hat{S}^{bot}$. This means the weighting factor $\hat{\omega}^{bot,LI7500}$ needs to be appropriately sized to account for the heat from all of the cylinder surfaces. While the a priori value of 0.108 might be too small to account for the heat flux from the sides, the 95% credible interval of 0.111 to 0.139 in our analysis indicates that it is not unreasonably underestimated.

The IRGA self-heating correction can be attributed to both the internal electronics and solar radiation absorbed by the sensor. As shown in Appendix B, when we modeled surface temperatures from meteorological variables, the bottom temperatures were predicted to be hotter with an older LI-7500 serial number. Based on personal communications with G. Burba, we hypothesize that this is attributed to the older unit having different solar absorption characteristics due to its older paint. Since our study used direct measurements of surface temperatures, it was not necessary to take this effect into account when revising the self-heating correction. Though for applications where surface temperatures are predicted with an empirical model, accounting for solar absorption and its interaction with different aged sensors in a manner similar to Appendix B might be reasonable.

4.3. Implications

Although the problems that we identify in the self-heating correction of Burba et al. (2008) approximately cancel out (i.e., $S_{B08}^{bot,LI7500}$ and $S_{B08}^{top,LI7500}$ are ~10 times too small while ω_{B08}^{bot} and ω_{B08}^{top} are ~10 times too large) and the resulting $\Delta S_{B08}^{surf,LI7500}$ are similar to $\Delta \hat{S}^{surf,LI7500}$ (Figs. 4f versus 5d, purple shading; Fig. 8a versus d; Table 2, ΔS^{surf} with

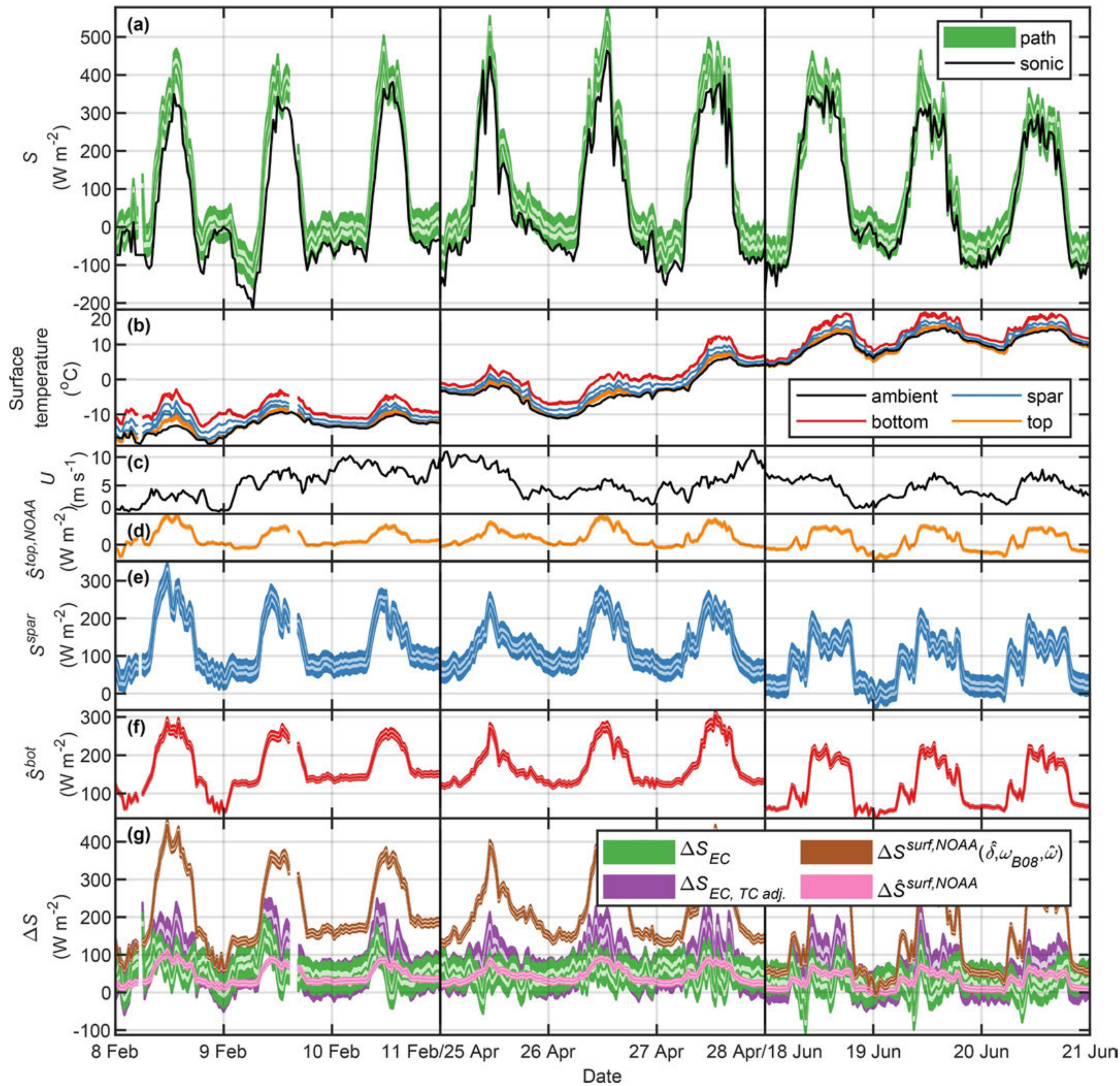

Fig. 9. An illustration of the NOAA IRGA self-heating correction. (a) Sensible heat flux was measured inside the path with thermocouples (S^{path}) and outside with a sonic anemometer (S^{sonic}). (b) Ambient and NOAA IRGA surface temperatures are combined with (c) wind speed (U) to estimate the surface heat fluxes (d) $\hat{S}^{top,NOAA}$, (e) S^{spar}, and (f) $\hat{S}^{bot}$. (g) Since S^{out} was not measured with thermocouples, ΔS_{EC} was calculated as S^{path} - S^{sonic} using original (green shading) and thermocouple adjusted (TC adj., purple shading) S^{path} measurements; ΔS was also estimated with a weighted sum of heat fluxes from key instrument surfaces (ΔS^{surf}) using ω_{B08}^{bot} and ω_{B08}^{top} defined a priori in Burba et al. (2008) and $\hat{\omega}^{spar,NOAA}$ defined by this study (Eq. 20, brown shading) and $\hat{\omega}^{NOAA}$ defined by this study (Eq. 19, pink shading). Shading (i.e. light/dark) represents the median, inner quartile range, and 95% credible interval of the posterior distribution for each process parameter and derived quantity. Panels a, d-g have the same vertical scaling.

mean ± standard deviation of 16.6 ± 21.3 W m^{-2} versus 20.1 ± 25.1 W m^{-2}, R^2 of 0.62 versus 0.66 when fitted to ΔS_{EC}), there are benefits to accurately describing the self-heating contribution from each of the IRGA surfaces. First, it is uncertain if these errors will balance at other field sites. Under the unusually windy conditions at GLEES (Frank et al., 2014) the differences in $S_{B08}^{bot,LI7500}$ and $\hat{S}^{bot,LI7500}$ were a factor of ~9. Yet, the differences between these two would be less pronounced for lower winds; for example, U = 1.0 m s^{-1} leads to a factor of ~5 difference. Also, the 4 mm and 4.5 mm boundary layer adjustment terms for non-flat surfaces suppress the influence of wind velocity and lead to smaller coefficients of variation in $S_{B08}^{bot,LI7500}$

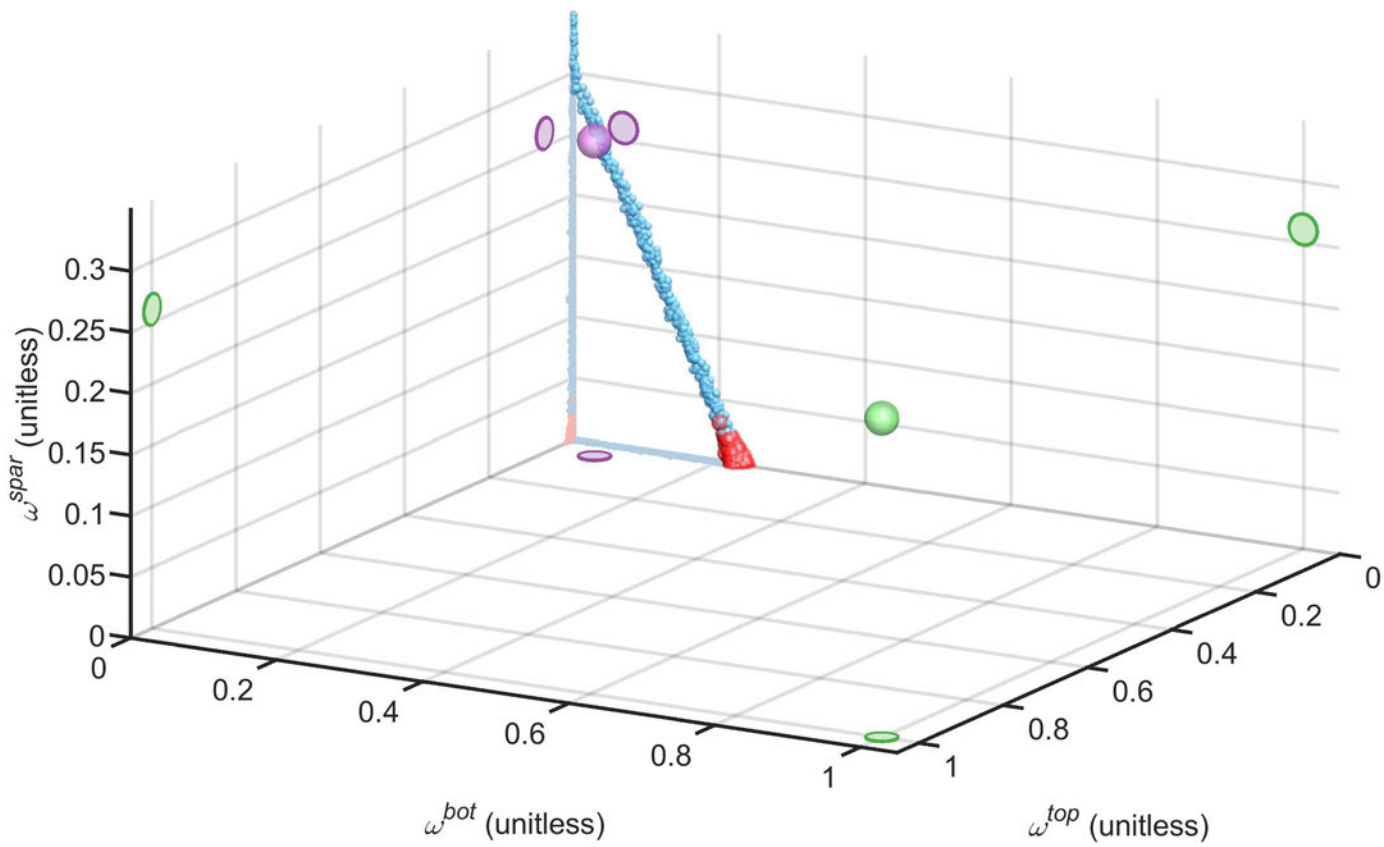

Fig. 10. Bayesian analysis of the weighted sum of surface heat fluxes (i.e., $\hat{S}^{bot}$, $\hat{S}^{top,NOAA}$, and S^{spar}) required to match the NOAA IRGA self-heating measured with eddy covariance (ΔS_{EC}). The green dot is the a priori weighting defined in Eq. 20 with parameters ω_{B08}^{bot} and ω_{B08}^{top} defined by Burba et al. (2008) and $\hat{\omega}^{spar,NOAA}$ defined by this study; these values were used to define the prior probability distributions in the Bayesian analyses. The purple dot is the a priori weighting defined by this study with $\hat{\omega}^{bot,NOAA}$ and $\hat{\omega}^{top,NOAA}$ in Eq. 19. The blue dots are plausible Bayesian posterior weightings obtained by applying the Bayesian cut function to the ω^{spar} parameter; the red dots are obtained without the Bayesian cut function. ΔS_{EC} was calculated using original (i.e. not thermocouple adjusted) S^{path} measurements.

and $S_{B08}^{top,LI7500}$. Thus, while the B08 correction and our proposed formulation both resulted in similar ΔS^{surf} at GLEES, this should not be expected elsewhere. Second, the methodology of Burba et al. (2008) is not universal and cannot be generalized to other IRGAs (e.g., it fails for the NOAA IRGA). Third, the role of the spar could be misinterpreted. Equation 3 implies that S^{spar} is 15% as important as S^{bot}. To the contrary, the spar is likely of equal if not more importance to the bottom (Table 2, for all but $\Delta S^{surf,LI7500}(\delta_{B08}, \hat{\omega})$ and $\Delta S^{surf,LI7500}(\hat{\delta}, \omega_{B08})$ where $\omega^{spar}S^{spar}$ had means between 8.1 to 12.2 W m^{-2} and standard deviations between 12.8 and 19.2 W m^{-2} compared to $\omega^{bot}S^{bot}$ which had means between 7.5 to 8.9 W m^{-2} and standard deviations between 5.2 and 6.0 W m^{-2}). A consequence of understating the importance of the spar is dealing with inclined sensors. Modifications to the self-heating correction for tilted IRGAs such as Oechel et al. (2014) focus only on the bottom and top surface temperatures. Yet, since the IRGA measurement volume is more exposed to the spars than to the bottom and top surfaces, the spar is likely the key surface for predicting the self-heating of an inclined IRGA. While the spars are often overlooked, in the LI-7500 they are warm due to the air that flows through them from the bottom, and our results show that the heat from the spar is far from negligible.

We doubt the universality of our Bayesian posterior weightings and whether it is appropriate to utilize them in other studies. These estimates were derived from experiments with IRGAs tilted 15° northward, with a strong westerly wind, and with surface and path temperatures measured using multiple thermocouples. We believe it is likely that a different IRGA orientation, field site, or measurement technology, e.g. path temperature measured with a fine-wire thermometer (Grelle and Burba, 2007), would yield different posterior weightings. Instead, we interpret our posterior weightings in the context of evidence to either retain or reject our hypothesis that a priori weighting factors based on the proportion of surface area that contributes heating are reasonable. As discussed, we retain our hypothesis, and therefore believe the most universal weightings for the revised self-heating correction for the LI-7500 is Eq. 14 and for the NOAA IRGA is Eq. 19.

The results of this study show that IRGA self-heating is considerable, particularly during the day, and especially during the winter, which is consistent with Burba et al. (2008). The bottom and spar surfaces remain warm (Fig. 4a) despite the high winds at GLEES (Fig. 3c) that might otherwise be predicted to convectively cool the IRGA surfaces. Technological improvements in the internal temperature of the LI-7500 series beginning with the LI-7500A likely reduce this problem (Burba, 2013). Other studies have investigated on the impact of the self-heating correction on the net ecosystem exchange of carbon dioxide in cold-weather environments (Amiro, 2010; Reverter et al., 2011; Wang et al., 2017a; Wang et al., 2017b). Though this is not our focus, our revised self-heating correction has been incorporated by Berryman et al. (2018) into a comparison between winter CO_2 respiration measured with eddy covariance versus snowpack CO_2 gradients at GLEES; their results indicated that the average winter CO_2 fluxes measured with the two methodologies were similar.

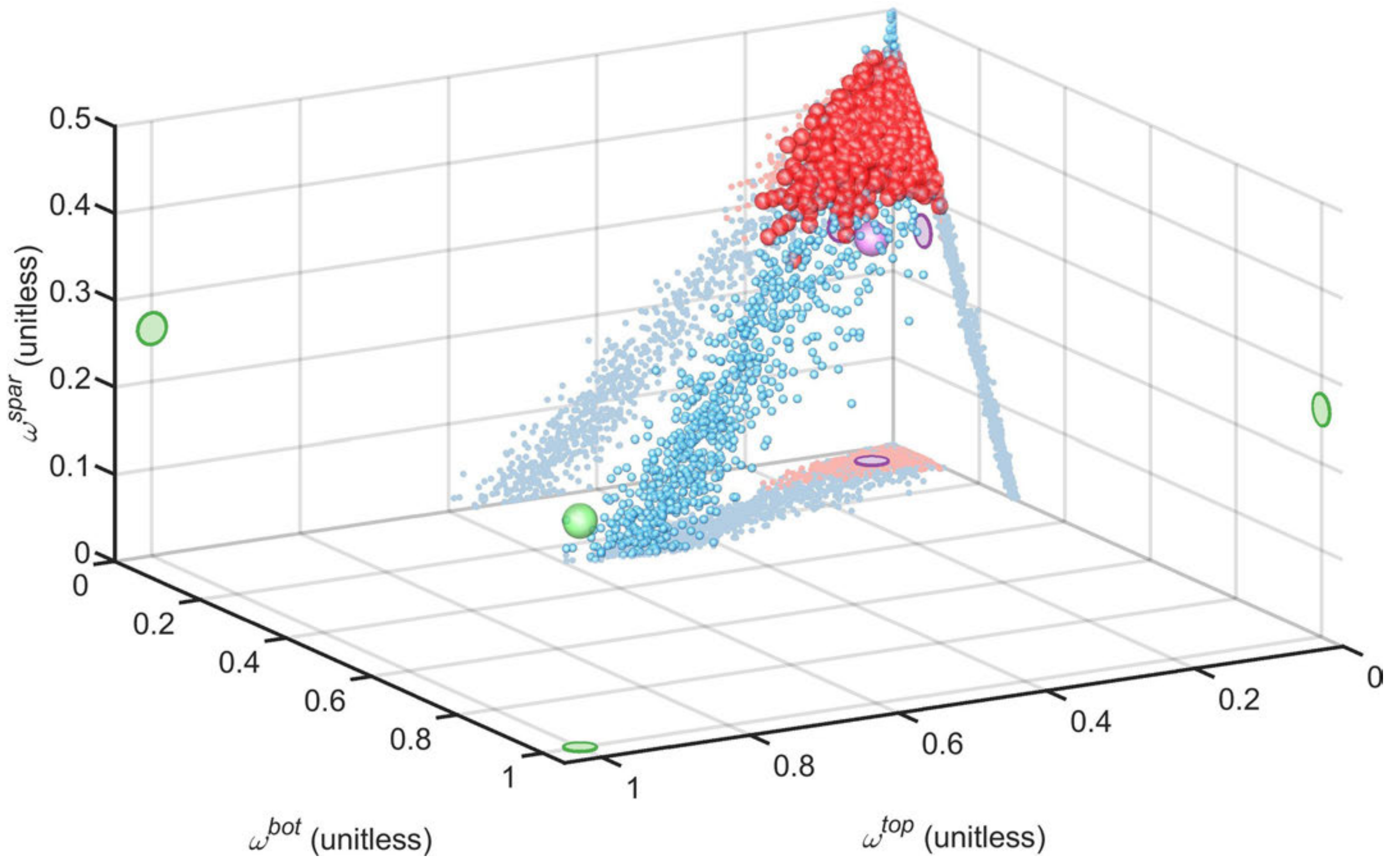

Fig. 11. The same as Fig. 10 for the NOAA IRGA, except since S^{out} was not measured, $\Delta S_{EC,TC\ adj.}$ was calculated as S^{path} - S^{sonic} using thermocouple adjusted S^{path} measurements.

Table 3
The additional heat flux, ΔS, from the NOAA IRGA measured via eddy covariance (EC) using thermocouples inside of the IRGA path (S^{path}) versus estimated with a weighted (ω^{bot}, ω^{top}, and ω^{spar}) sum of heat fluxes from key instrument surfaces (S^{bot}, S^{top}, and S^{spar}). Since S^{out} was not measured, ΔS_{EC} was calculated as S^{path} - S^{sonic} using original and thermocouple adjusted (TC adj.) S^{path} measurements. Four weightings were implemented (ω_{N08} a priori similar to Burba et al. (2008), $\hat{\omega}^{NOAA}$ a priori from this study, and the Bayesian posteriors that predict ΔS_{EC} and $\Delta S_{EC,TC\ adj.}$ from the surface heat fluxes). The Bayesian posterior weighting parameters are summarized as median (95% Bayesian credible interval); random effect parameters are not reported. The derived quantities for ΔS and the surface heat fluxes have posterior distributions which are summarized as mean ± standard deviation.

Measurement	Surface heat flux weighting	ω^{bot} (unitless)	ω^{top} (unitless)	ω^{spar} (unitless)	$\omega^{bot}S^{bot}$ (W m^{-2})	$\omega^{top}S^{top}$ (W m^{-2})	$\omega^{spar}S^{spar}$ (W m^{-2})	ΔS (W m^{-2})
EC	-	-	-	-	-	-	-	39.3 ± 36.7
EC, TC adjusted	-	-	-	-	-	-	-	57.1 ± 48.8
IRGA surface temperature	ω_{B08}, $\hat{\omega}^{NOAA}$	1	1	0.261	165.3 ± 56.5	19.8 ± 24.2	32.3 ± 16.7	217.4 ± 94.7
	$\hat{\omega}^{NOAA}$	0.069	0.069	0.261	11.4 ± 3.9	1.4 ± 1.7	32.3 ± 16.7	45.0 ± 21.9
	$\omega_{posterior}$ fit to ΔS_{EC}	0.228 (0.215–0.236)	0.001 (0.000–0.007)	0.003 (0.000–0.017)	37.6 ± 12.9	0.0 ± 0.0	0.4 ± 0.2	38.1 ± 13.1
	$\omega_{posterior}$ fit to $\Delta S_{EC,TC\ adj.}$	0.061 (0.020–0.098)	0.032 (0.001–0.158)	0.373 (0.319–0.427)	10.0 ± 3.4	0.6 ± 0.8	46.1 ± 23.8	56.9 ± 28.0

In summary, we conclude that significant IRGA self-heating exists in a cold, windy, high elevation, mountainous field site. We determined that the self-heating correction of Burba et al. (2008) contains two significant errors: (1) unwarranted boundary layer adjustment terms for non-flat surfaces which result in surface heat fluxes that are an order of magnitude less than is reasonable and (2) bottom and top surface heat flux weightings are improbable and are an order of magnitude too large. Though these errors roughly canceled out at our field site, this generally should not be expected elsewhere. Thus, we believe a revised formulation for the self-heating correction is justified, as described for the LI-7500 in Eqs. 8–14. A new formulation emphasizes the role of the spar in self-heating, which should be taken into consideration for all cold-weather installations, regardless of the IRGA tilt angle. Finally, we describe a simple and pragmatic methodology for measuring surface temperatures with thermocouples, which would allow for improved estimates of the IRGA self-heating effect for other field sites. These recommendations should improve the quality of eddy-covariance measurements in current or future deployments along with archival data.

Declaration of Competing Interest

The authors declare that they have no known competing financial interests or personal relationships that could have appeared to influence the work reported in this paper.

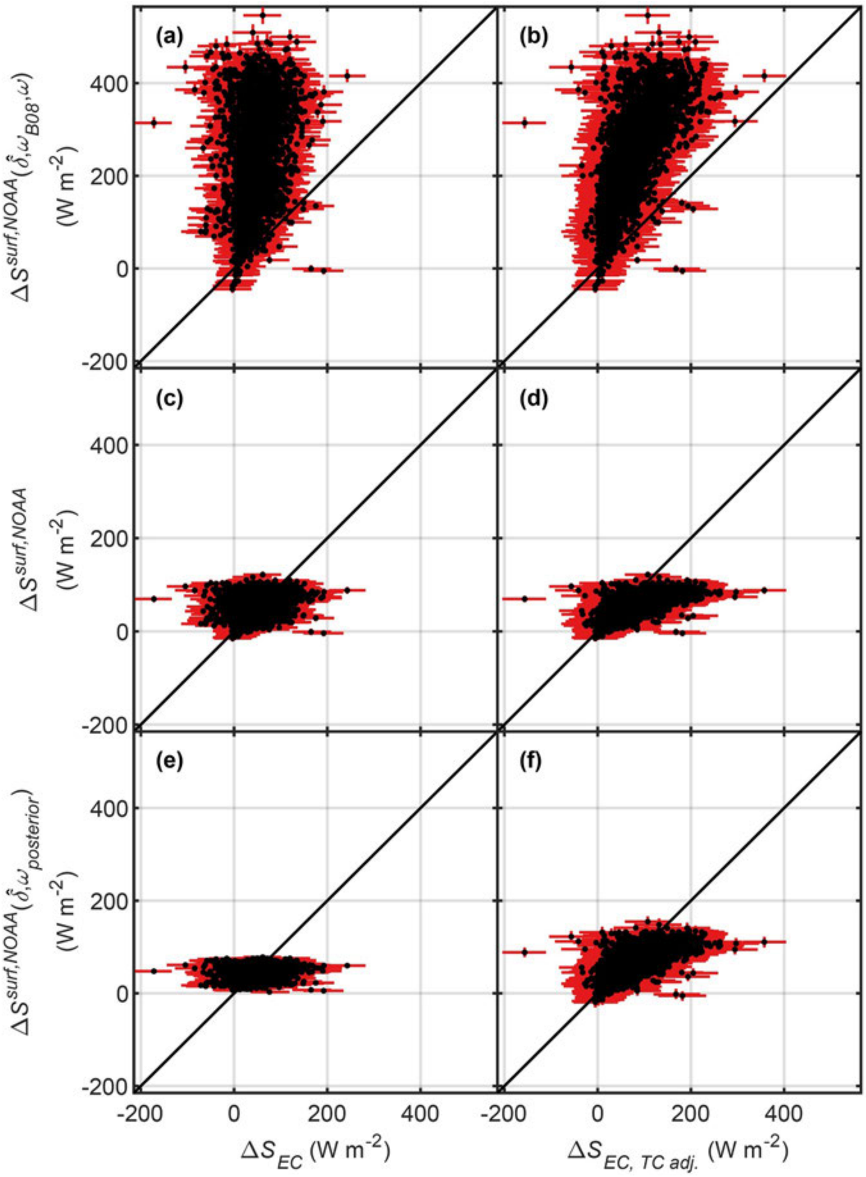

Fig. 12. Comparisons of the additional heat flux in the NOAA IRGA path, ΔS, for each half-hour measured via eddy covariance (EC) using thermocouples inside of the IRGA path versus estimated with a weighted sum of heat fluxes from key instrument surfaces (ΔS^{surf}). Since S^{out} was not measured, ΔS_{EC} was calculated as S^{path} - S^{sonic} using (a, c, e) original and (b, d, f) thermocouple adjusted (TC adj.) S^{path} measurements. The weighting parameters in (a-b) include ω_{B08}^{bot} and ω_{B08}^{top} defined a priori in Burba et al. (2008) (Eq. 20), in (c-d) are $\hat{\omega}^{NOAA}$ defined a priori in this study (Eq. 19), and in (e-f) are the Bayesian posteriors that most likely predict (e) ΔS_{EC} and (f) $\Delta S_{EC,\ TC\ adj}$. The red shading represents the 95% credible interval of the posterior distribution for each derived quantity.

Acknowledgements

We thank George Burba for his interaction with us on this topic. We thank Werner Eugster and two anonymous reviewers whose thoughtful comments improved this manuscript. This study was funded by the USDA Forest Service.

Appendix A. Bayesian prior distributions

This is a complete list of all process parameters and their prior distributions used in the various analyses.

For the first analysis of the LI-7500 (i.e., detecting sensible heat flux within the measurement path), the following statistical process parameters were defined with prior probability distributions (either normal, gamma, or uniform with expected value, E, and standard deviation, σ): S^{out} (uniform between maximum and minimum of S data in W m^{-2}, defined for each half-hour); the fixed effects b_{day}, b_{night}, $b_{day,U}$, $b_{night,U}$, $b_{day,Ta}$, and $b_{day,\theta}$ (normal, E = 0 W m^{-2}, σ = 20 W m^{-2}), m_{day} and m_{night} (normal, E = 1, σ = 0.2), $m_{day,U}$, $m_{night,U}$, $m_{day,Ta}$, $m_{day,\theta}$, and $m_{night,\theta}$ (normal, E = 0, σ = 0.05); the random effects $\sigma_{b,path}$ and $\sigma_{b,out}$ (gamma, E = 20 W m^{-2}, σ = 20 W m^{-2}), $\sigma_{m,path}$ and $\sigma_{m,out}$ (gamma, E = 0.05, σ = 0.05), $b_{path,1}$, $b_{path,2}$, and $b_{path,3}$ (normal, E = 0, $\sigma = \sigma_{b,path}$), $b_{out,1}$, $b_{out,2}$, and $b_{out,3}$ (normal, E = 0, $\sigma = \sigma_{b,out}$), $m_{path,1}$, $m_{path,2}$, and $m_{path,3}$ (normal, E = 0, $\sigma = \sigma_{m,path}$), $m_{out,1}$, $m_{out,2}$, and $m_{out,3}$ (normal, E = 0, $\sigma = \sigma_{m,out}$); and $\sigma_{prediction}$ (gamma, E = 1% of range of S data in W m^{-2}, σ = 1% of range of S data in W m^{-2}) and $\eta_{heteroscedasticity}$ (gamma, E = 1/(20% of range of S data) in W^{-1} m^2, σ = 1/(20% of range of S data) in W^{-1} m^2). The standard deviations of these normal distributions were a single process parameter, $\sigma_{prediction}$, adjusted for heteroscedasticity in the magnitude of the predicted heat flux, i.e. $\sigma_{prediction}(1 + \eta_{heteroscedasticity}|S|)$.

Table A1
Parameters for an empirical model similar to Table 2 in Burba et al. (2008), predicting half-hourly LI-7500 surface temperatures from ambient meteorology at GLEES based on multiple regression using forward stepwise model selection from among various meteorological variables. The differences in surface temperatures and ambient air temperature, T_s - T_a, are predicted by an offset (dependent on instrument serial number and category of wind direction θ), air temperature (T_a,°C), down-welling short-wave radiation ($R_{s\downarrow}$, W m^{-2}, daytime only), upwelling long-wave radiation ($R_{l\uparrow}$, W m^{-2}, nighttime only), wind speed (U, m s^{-1}), and temperature covariance ($\overline{w'T_a'}$, K m s^{-1}). At GLEES, sensors were on a boom mounted at 270° from the scaffold. Sensor S/N 1751 was not included because the top surface temperatures were not measure during its installation.

		Offset (°C)						
		S/N 0235	S/N 1259	345° ≤ θ < 15°	15° ≤ θ < 45°	45° ≤ θ < 75°	75° ≤ θ < 105°	105° ≤ θ < 135°
Daytime	T_s^{bot} - T_a	3.23	2.57	-0.06	0.35	0.88	1.37	1.04
	T_s^{top} - T_a		0.37	-0.11	0.02	0.43	0.91	1.23
	T_s^{spar} - T_a		1.01	0.16	0.36	0.72	1.27	0.81
Nighttime	T_s^{bot} - T_a	-9.05	-9.75	-0.09	-0.02	0.17	0.50	0.51
	T_s^{top} - T_a		-13.26	0.08	0.38	0.85	1.39	0.94
	T_s^{spar} - T_a		-10.11	-0.07	0.04	0.30	0.69	0.74

	Offset (°C)						
	135° ≤ θ < 165°	165° ≤ θ < 195°	195° ≤ θ < 225°	225° ≤ θ < 255°	255° ≤ θ < 285°	285° ≤ θ < 315°	315° ≤ θ < 345°
Daytime	0.65	0.10	0.06	0.00	-0.06	0.00	0.10
	0.62	0.54	0.13	0.00	-0.14	-0.31	-0.32
	0.47	0.04	0.05	0.00	0.03	0.16	0.23
Nighttime	0.30	0.28	0.01	0.00	-0.02	-0.09	-0.14
	0.60	0.14	0.04	0.00	0.01	0.14	0.20
	0.41	0.37	0.03	0.00	-0.04	-0.14	-0.15

		Parameter 1 (for T_a) (unitless)	Parameter 2 (for $R_{s\downarrow}$) (°C W^{-1} m^2)	Parameter 3 (for $R_{l\uparrow}$) (°C W^{-1} m^2)	Parameter 4 (for U) (°C m^{-1} s)	Parameter 5 (for) (m^{-1} s)
Daytime	T_s^{bot} - T_a	-0.0494	-0.002289	-	-0.2000	5.906
	T_s^{top} - T_a	0.0005	-0.002788	-	0.0240	4.341
	T_s^{spar} - T_a	-0.0037	-0.003062	-	-0.0320	5.234
Nighttime	T_s^{bot} - T_a	-0.2387	-	0.03805	-0.2018	2.508
	T_s^{top} - T_a	-0.1850	-	0.04240	0.0356	2.963
	T_s^{spar} - T_a	-0.1643	-	0.03391	-0.0231	2.698

For the second analysis of the LI-7500 (i.e., the effect of boundary layer definitions and weightings on the accuracy of the sum of surface heat fluxes), in the first step the following statistical process parameters were defined with prior probability distributions: S^{path}, S^{out}, $S_{B08}^{bot,LI7500}$, $\hat{S}^{bot}$, $S_{B08}^{top,LI7500}$, $\hat{S}^{top,LI7500}$, and S^{spar} (uniform between maximum and minimum of S data in W m^{-2}, defined for each half-hour); the random effects, which were applied separately for the seven S, were σ_b (gamma, E = 0.1 W m^{-2}, σ = 0.1 W m^{-2}), σ_m (gamma, E = 0.1, σ = 0.1), b_{rep1}, b_{rep2}, and b_{rep3} (normal, E = 0, $\sigma = \sigma_b$), m_{rep1}, m_{rep2}, and m_{rep3} (normal, E = 0, $\sigma = \sigma_m$); and $\sigma_{prediction}$ (gamma, E = 1% of range of S data in W m^{-2}, σ = 1% of range of S data in W m^{-2}) and $\eta_{heteroscedasticity}$ (gamma, E = 1/(20% of range of S data) in W^{-1} m^2, σ = 1/(20% of range of S data) in W^{-1} m^2) which were applied together for S^{path} and S^{out} but separately for the other five S. In the second step the following statistical process parameters were defined with prior probability distributions: the fixed effects ω^{bot} (gamma, E = 1, σ = 1), ω^{top} (gamma, E = 1, σ = 1), and ω^{spar} (gamma, E = 0.15, σ = 0.15), $\sigma_{prediction}$ (gamma, E = 1% of range of S data in W m^{-2}, σ = 1% of range of S data in W m^{-2}), and $\eta_{heteroscedasticity}$ (gamma, E = 1/(20% of range of S data) in W^{-1} m^2, σ = 1/(20% of range of S data) in W^{-1} m^2).

The NOAA analyses was similar to the second analysis of the LI-7500 except these process parameters which were defined with prior probability distributions: S^{path}, $\hat{S}^{bot}$, $\hat{S}^{top,NOAA}$, and S^{spar} (uniform between maximum and minimum of S data in W m^{-2}, defined for each half-hour) and ω^{spar} (gamma, E = 0.261, σ = 0.261).

Appendix B. Predicting half-hourly LI-7500 surface temperatures from ambient meteorology

Though the analyses in this paper are based on thermocouple measurements of IRGA surface temperatures, it is useful to predict surface temperatures from ambient meteorology. An empirical model was developed for the GLEES site for the LI-7500 similar to Table 2 in Burba et al. (2008). Predictor variables were chosen from among the standard meteorological measurements in the GLEES AmeriFlux dataset (http://ameriflux.lbl.gov/) as described by Frank et al. (2014). Forward stepwise model selection was used to include predictors that were statistically significant. Similar to Burba et al. (2008), this empirical model predicted LI-7500 surface temperatures from ambient air temperature, down-welling short-wave radiation during daytime, upwelling long-wave radiation during nighttime, and wind velocity (Table A1). In addition, this model included the vertical temperature covariance as well as categorical variables for IRGA serial number and wind direction (Table A1). The IRGA serial number can account for the ages of the sensor and how the reflectivity of their exterior paint can change, affecting the absorbance of solar energy. The wind direction can account for the tower and mounting structures and their effects on cooling of the IRGA.

References

Amiro, B., 2010. Estimating annual carbon dioxide eddy fluxes using open-path analysers for cold forest sites. Agricultural and Forest Meteorol. 150 (10), 1366–1372.
Amiro, B.D., et al., 2010. . Ecosystem carbon dioxide fluxes after disturbance in forests of North America. J. Geophys. Res. 115, G00K02.
Auble, D.L., Meyers, T.P., 1992. An open path, fast response infrared absorption gas analyzer for H2O and CO2. Boundary-Layer Meteorol. 59 (3), 243–256.
Baldocchi, D., 2014. Measuring fluxes of trace gases and energy between ecosystems and the atmosphere – the state and future of the eddy covariance method. Global Change Biol. 20 (12), 3600–3609.
Berryman, E.M., Frank, J.M., Massman, W.J., Ryan, M.G., 2018. Using a Bayesian framework to account for advection in seven years of snowpack CO2 fluxes in a mortality-impacted subalpine forest. Agricultural and Forest Meteorol. 249, 420–433.
Blanken, P.D., et al., 2009. . A comparison of water and carbon dioxide exchange at a windy alpine tundra and subalpine forest site near Niwot Ridge, Colorado. Biogeochemistry 95 (1), 61–76.
Brown, M., et al., 2010. . Impact of mountain pine beetle on the net ecosystem production of lodgepole pine stands in British Columbia. Agricultural and Forest Meteorology 150 (2), 254–264.
Burba, G., 2013. Eddy covariance method. Li-COR Biogeosciences, Lincoln, NE.
Burba, G., Anderson, D., Xu, L. and McDermitt, D., 2006. Correcting apparent off-season CO2 uptake due to surface heating of an open path gas analyzer: progress report of an ongoing study, proceedings of 27th Annual Conference of Agricultural and Forest Meteorology, San Diego, California, 13pp.
Burba, G.G., McDermitt, D.K., Grelle, A., Anderson, D.J., Xu, L.K., 2008. Addressing the influence of instrument surface heat exchange on the measurements of CO2 flux from open-path gas analyzers. Global Change Biol. 14 (8), 1854–1876.
Euskirchen, E., Bret-Harte, M.S., Scott, G., Edgar, C., Shaver, G.R., 2012. Seasonal patterns of carbon dioxide and water fluxes in three representative tundra ecosystems in northern Alaska. Ecosphere 3 (1), 1–19.
Euskirchen, E., Bret-Harte, M.S., Shaver, G.R., Edgar, C.W., Romanovsky, V., 2017. Long-term release of carbon dioxide from arctic tundra ecosystems in Alaska. Ecosystems 20 (5), 960–974.
Frank, J.M., Massman, W.J., Ewers, B.E., Huckaby, L.S., Negrón, J.F., 2014. Ecosystem CO2/H2O fluxes are explained by hydraulically limited gas exchange during tree mortality from spruce bark beetles. J. Geophys. Res.: Biogeosci. 119 (6), 1195–1215.
Frank, J.M., Massman, W.J., Ewers, B.E., Williams, D.G., 2019. Bayesian analyses of 17 winters of water vapor fluxes show bark beetles reduce sublimation. Water Resources Res. 55 (2), 1598–1623.
Galvagno, M., et al., 2013. . Phenology and carbon dioxide source/sink strength of a subalpine grassland in response to an exceptionally short snow season. Environmental Res. Lett. 8 (2), 025008.
Goodrich, S.S., Marcum, W.R., 2019. Natural convection heat transfer and boundary layer transition for vertical heated cylinders. Experimental Thermal and Fluid Sci. 105, 367–380.
Grelle, A., Burba, G., 2007. Fine-wire thermometer to correct CO2 fluxes by open-path analyzers for artificial density fluctuations. Agricultural and Forest Meteorol. 147 (1-2), 48–57.
Hobbs, N.T., Hooten, M.B., 2015. Bayesian models: a statistical primer for ecologists. Princeton University Press.
Holl, D., et al., 2019. . A long-term (2002 to 2017) record of closed-path and open-path eddy covariance CO2 net ecosystem exchange fluxes from the Siberian Arctic. Earth System Sci. Data 11 (1), 221–240.
Huang, G., 2015. Numerical simulation of solid particle transport in atmospheric boundary-layer over obstacles. PhD. Dissertation. Ecully Ecole centrale de Lyon.
Ikawa, H., Faloona, I., Kochendorfer, J., Paw, U., Oechel, W., 2013. Air–sea exchange of CO2 at a Northern California coastal site along the California current upwelling system. Biogeosciences 10 (7), 4419–4432.
Järvi, L., et al., 2009. . Comparison of net CO2 fluxes measured with open- and closed-path infrared gas analyzers in an urban complex environment. Boreal Environment Res. 14, 499–514.
Kittler, F., et al., 2017. . High-quality eddy-covariance CO2 budgets under cold climate conditions. J. Geophy. Res.: Biogeosciences 122 (8), 2064–2084.
Kruschke, J., 2014. Doing Bayesian data analysis: A tutorial with R, JAGS, and Stan. Academic Press.
Lafleur, P.M., Humphreys, E.R., 2018. Tundra shrub effects on growing season energy and carbon dioxide exchange. Environmental Res. Lett. 13 (5), 055001.
Lee, X., Finnigan, J.J., Paw U, K.T., 2004. Coordinate system and flux bias error. In: Lee, X., Massman, W.J., Law, B.E. (Eds.), Handbook of micrometeorology. Kluwer Academic Publishers, Dordrecht, The Netherlands, pp. 33–66.
Lee, X., Massman, W.J., 2011. A perspective on thirty years of the Webb. Pearman and Leuning density corrections 139 (1), 37–59 Boundary-Layer Meteorology.
Lu, D., Ye, M., Hill, M.C., 2012. Analysis of regression confidence intervals and Bayesian credible intervals for uncertainty quantification. Water Resources Res. 48 (9), W09521.
Lüers, J., Westermann, S., Piel, K., Boike, J., 2014. Annual CO2 budget and seasonal CO2 exchange signals at a high Arctic permafrost site on Spitsbergen, Svalbard archipelago. Biogeosciences 11 (22), 6307–6322.
Marushchak, M., et al., 2013. . Carbon dioxide balance of subarctic tundra from plot to regional scales. Biogeosciences.
Massman, W.J., 2000. A simple method for estimating frequency response corrections for eddy covariance systems. Agricultural and Forest Meteorol. 104 (3), 185–198.
Massman, W.J., Lee, X., 2002. Eddy covariance flux corrections and uncertainties in long-term studies of carbon and energy exchanges. Agricultural and Forest Meteorol. 113 (1-4), 121–144.
Mathys, A., et al., 2013. . Carbon balance of a partially harvested mixed conifer forest following mountain pine beetle attack and its comparison to a clear-cut. Biogeosciences 10 (8), 5451–5463.
Meek, D.W., Prueger, J.H., Sauer, T.J., 1998. Solutions for three regression problems commonly found in meteorological data analysis. In: Strand, J.F., Goens, D.W. (Eds.), 23rd Conference on Agricultural Forest Meteorology. American Meteorological Society, Albuquerque, NM, pp. 141–145.
Miller, L.A., et al., 2011. . Carbon dynamics in sea ice: A winter flux time series. J. Geophys. Res.: Oceans 116 (C2).
Musselman, R.C., 1994. The Glacier Lakes Ecosystem Experiments Site. USDA Forest Service, Fort Collins, CO Rocky Mountain Forest and Range Experiment Station.

Nash, J.E., Sutcliffe, J.V., 1970. River flow forecasting through conceptual models part I—A discussion of principles. J. Hydrol. 10 (3), 282–290.
Neiswanger, W., Wang, C., Xing, E.P., 2014. Asymptotically exact, embarrassingly parallel MCMC. Proceedings of the Thirtieth Conference on Uncertainty in Artificial Intelligence. AUAI Press, Quebec City, Quebec, Canada, pp. 623–632.
Nobel, P.S., 1983. Biophysical plant physiology and ecology. W. H. Freeman and Company, San Francisco, CA, pp. 608.
Nordbo, A., Järvi, L., Vesala, T., 2012. Revised eddy covariance flux calculation methodologies–effect on urban energy balance. Tellus B: Chemical and Physical Meteorol. 64 (1), 18184.
Oechel, W.C., Laskowski, C.A., Burba, G., Gioli, B., Kalhori, A.A., 2014. Annual patterns and budget of CO2 flux in an Arctic tussock tundra ecosystem. J. Geophys. Res.: Biogeosciences 119 (3), 323–339.
Ono, S., et al., 2014. . Measurement of a doubly substituted methane isotopologue, 13CH3D, by tunable infrared laser direct absorption spectroscopy. Analytical Chemistry 86 (13), 6487–6494.
Plummer, M., 2003. JAGS: A program for analysis of Bayesian graphical models using Gibbs sampling, Proceedings of the 3rd International Workshop on Distributed Statistical Computing (DSC 2003) March 20–22, Vienna, Austria. Technische Universit at Wien. Vienna, Austria.
… InPlummer, M., 2011. generating data from a stochastic model. Editor In: Plummer, M (Ed.), JAGS: Just Another Gibbs Sampler. Sourceforge.
Plummer, M., 2015a. Cuts in Bayesian graphical models. Statistics and Computing 25 (1), 37–43.
Plummer, M., 2015b. rjags: Bayesian graphical models using MCMC, version 4-4. R package. URLhttp://CRAN.R-project.org/package=rjags.
Plummer, M., Best, N., Cowles, K., Vines, K., 2006. CODA: Convergence Diagnosis and Output Analysis for MCMC. R News 6. R Foundation, Vienna, Austria, pp. 7–11. URL. https://www.r-project.org/doc/Rnews/Rnews_2006-1.pdf.
Core Team, R, 2015. R: A language and environment for statistical computing. R Foundation for Statistical Computing, Vienna, Austria URL. https://www.R-project.org/.
Reverter, B.R., et al., 2011. . Adjustment of annual NEE and ET for the open-path IRGA self-heating correction: Magnitude and approximation over a range of climate. Agricultural and Forest Meteorol. 151 (12), 1856–1861.
Rogiers, N., Conen, F., Furger, M., Stoeckli, R., Eugster, W., 2008. Impact of past and present land-management on the C-balance of a grassland in the Swiss Alps. Global Change Biol. 14 (11), 2613–2625.
Rosenthal, J.S., 2000. Parallel computing and Monte Carlo algorithms. Far East J. Theoretical Statistics 4 (2), 207–236.
Team, RStudio, 2015. RStudio: Integrated Development for R. RStudio, Inc., Boston, MA URL. http://www.rstudio.com/.
Senapati, J.R., Dash, S.K., Roy, S., 2017. Numerical investigation of natural convection heat transfer from vertical cylinder with annular fins. Int. J.Thermal Sci. 111, 146–159.
Spiegelhalter, D.J., Best, N.G., Carlin, B.P., Van Der Linde, A., 2002. Bayesian measures of model complexity and fit. J. Royal Statistical Society: Series B (Statistical Methodology) 64 (4), 583–639.
Sturtevant, C.S., Oechel, W.C., 2013. Spatial variation in landscape-level CO2 and CH4 fluxes from arctic coastal tundra: influence from vegetation, wetness, and the thaw lake cycle. Global Change Biol. 19 (9), 2853–2866.
Ueyama, M., et al., 2012. . Influences of various calculation options on heat, water and carbon fluxes determined by open-and closed-path eddy covariance methods. Tellus B: Chemical and Physical Meteorol. 64 (1), 19048.
Vanclay, J.K., Skovsgaard, J.P., 1997. Evaluating forest growth models. Ecological Modelling 98 (1), 1–12.
Vickers, D., Mahrt, L., 1997. Quality control and flux sampling problems for tower and aircraft data. J. Atmospheric and Oceanic Technol. 14 (3), 512–526.
Wang, L., et al., 2017a. . A meta-analysis of open-path eddy covariance observations of apparent CO2 flux in cold conditions in FLUXNET. J. Atmospheric and Oceanic Technol. 34 (11), 2475–2487.
Wang, X., Wang, C., Bond-Lamberty, B., 2017b. Quantifying and reducing the differences in forest CO2-fluxes estimated by eddy covariance, biometric and chamber methods: A global synthesis. Agricultural and Forest Meteorol. 247, 93–103.
Webb, E.E., et al., 2016. . Increased wintertime CO2 loss as a result of sustained tundra warming. J. Geophysical Res.: Biogeosci. 121 (2), 249–265.
Webb, E.K., Pearman, G.I., Leuning, R., 1980. Correction of flux measurements for density effects due to heat and water vapour transfer. Quart.J.Royal Meteorological Society 106 (447), 85–100.
Wilkinson, D.J., Kontoghiorghes, E.J, 2006. Parallel bayesian computation. Editor. Handbook of Parallel Computing and Statistics. Chapman & Hall/CRC, Boca Raton, FL, pp. 481–512.
Willman, C., Ewart, P., 2016. Multipoint temperature measurements in gas flows using 1-D laser-induced grating scattering. Experiments in Fluids 57 (12), 191.
Wood, N., 1995. The onset of separation in neutral, turbulent flow over hills. Boundary-Layer Meteorol. 76 (1-2), 137–164.
Zweifel, R., et al., 2010. . Link between continuous stem radius changes and net ecosystem productivity of a subalpine Norway spruce forest in the Swiss Alps. New Phytologist 187 (3), 819–830.